

THEORETICAL STUDY OF ETHYLENE POLYMERIZATION BY PHENOXY-IMINE CATALYSTS



A Dissertation Submitted in Partial Fulfillment of the Requirements
for the Degree of Doctor of Philosophy in Chemistry

Department of Chemistry

FACULTY OF SCIENCE

Chulalongkorn University

Academic Year 2021

Copyright of Chulalongkorn University

การศึกษาเชิงทฤษฎีของพอลิเมอร์เซชันของเอทิลีนด้วยตัวเร่งปฏิกิริยาฟีนอกซีอิมิน



วิทยานิพนธ์นี้เป็นส่วนหนึ่งของการศึกษาตามหลักสูตรปริญญาวิทยาศาสตรดุษฎีบัณฑิต

สาขาวิชาเคมี ภาควิชาเคมี

คณะวิทยาศาสตร์ จุฬาลงกรณ์มหาวิทยาลัย

ปีการศึกษา 2564

ลิขสิทธิ์ของจุฬาลงกรณ์มหาวิทยาลัย

Thesis Title THEORETICAL STUDY OF ETHYLENE POLYMERIZATION BY
PHENOXY-IMINE CATALYSTS
By Mr. Pavee Apilardmongkol
Field of Study Chemistry
Thesis Advisor Professor VUDHICHAJ PARASUK, Ph.D.

Accepted by the FACULTY OF SCIENCE, Chulalongkorn University in Partial
Fulfillment of the Requirement for the Doctor of Philosophy

..... Dean of the FACULTY OF SCIENCE
(Professor POLKIT SANGVANICH, Ph.D.)

DISSERTATION COMMITTEE

..... Chairman
(Assistant Professor VARAWUT TANGPASUTHADOL, Ph.D.)

..... Thesis Advisor
(Professor VUDHICHAJ PARASUK, Ph.D.)

..... Examiner
(Associate Professor Somsak Pianwanit, Ph.D.)

..... Examiner
(Junjuda Unruangsri, Ph.D.)

..... External Examiner
(Chompoonut Rungnim, Ph.D.)

ปวีร์ อภิลาศมมงคล : การศึกษาเชิงทฤษฎีของพอลิเมอไรเซชันของเอทิลีนด้วยตัวเร่งปฏิกิริยาฟีนอกซีอิมิน. (THEORETICAL STUDY OF ETHYLENE POLYMERIZATION BY PHENOXY-IMINE CATALYSTS) อ.ที่ปรึกษาหลัก : ศ. ดร. วุฒิชัย พาราสุข

ในงานวิจัยนี้ ได้มีการศึกษากลไกการเกิดปฏิกิริยาเอทิลีนพอลิเมอไรเซชัน ด้วยตัวเร่งปฏิกิริยาฟีนอกซีอิมินและตัวเร่งปฏิกิริยานิกเกิลฟีนอกซีฟอสฟิน-โพลีเอทิลีนไกลคอลที่มีโลหะอัลคาไลน์ โดยใช้การคำนวณด้วยทฤษฎีฟังก์ชันนอลความหนาแน่นสำหรับตัวเร่งปฏิกิริยาฟีนอกซีอิมิน เมื่อศึกษาผลของการแทนที่ด้วยโลหะหมู่4B พบว่า แนวโน้มของค่าพลังงานกระตุ้นที่ได้จากการคำนวณในขั้นกำหนดอัตราเมื่อโลหะเป็น เซอร์โคเนียม < แอฟเนียม < ทาทาเนียม สอดคล้องกับผลการทดลอง เมื่อศึกษาผลของการเปลี่ยนหมู่แทนที่ของลิแกนด์ โดยเปลี่ยนไนโตรเจนอะตอมเป็นออกซิเจน หรือ ฟอสฟอรัส หรือ ซัลเฟอร์ ในกรณีโลหะไททาเนียม พบว่า การเปลี่ยนหมู่แทนที่เป็นซัลเฟอร์จะให้ค่าพลังงานกระตุ้นต่ำที่สุด ในกรณีโลหะเป็นนิกเกิล พบว่า รูปแบบโครงสร้างสารประกอบเชิงซ้อนเปลี่ยนแปลงไป โดยรูปทรงสี่เหลี่ยมจัตุรัสแบนราบ (square planar) เกิดปฏิกิริยาได้ดีกว่ารูปทรงแปดหน้า (octahedral) สำหรับตัวเร่งปฏิกิริยานิกเกิลฟีนอกซีฟอสฟิน-โพลีเอทิลีนไกลคอลที่มีโลหะอัลคาไลน์ เมื่อใช้โลหะอัลคาไลน์ต่างกัน 4 ระบบ พบแนวโน้มของค่าพลังงานกระตุ้นเมื่อใช้โลหะชนิดที่สอง ลิเทียม < โซเดียม < โพแทสเซียม < ซีเซียม ซึ่งสอดคล้องกับผลการทดลอง เมื่อศึกษาบทบาทของโลหะชนิดที่สองหรือโลหะอัลคาไลน์ ในตัวเร่งปฏิกิริยานิกเกิลฟีนอกซีฟอสฟิน-โพลีเอทิลีนไกลคอล โดยพิจารณาผลของความเกะกะ, อิเล็กทรอนิกส์ และไฟฟ้าสถิต จากการวิเคราะห์ด้วย DFT พบว่า ในตัวเร่งปฏิกิริยาที่ใช้โลหะสองชนิด ถ้าอันตรกิริยาระหว่างโลหะ-โลหะ/โลหะ-ลิแกนด์มีความแข็งแรงมาก และประจุของโลหะชนิดที่สองมีค่าเป็นบวกต่ำๆ จะช่วยเพิ่มอัตราการเกิดปฏิกิริยาได้ดี เมื่อศึกษาผลของโครงสร้างที่มีต่อค่าแอกติเวตี้ สามารถนำความสัมพันธ์ที่ได้ไปใช้ในการออกแบบตัวเร่งปฏิกิริยาใหม่ที่มีโลหะอัลคาไลน์เอิร์ธเป็นโลหะชนิดที่สอง งานวิจัยนี้จะให้ข้อมูลและรายละเอียดพื้นฐาน ในเรื่องการศึกษาปฏิกิริยาเอทิลีนพอลิเมอไรเซชัน โดยใช้ตัวเร่งปฏิกิริยาฟีนอกซีอิมินและตัวเร่งปฏิกิริยานิกเกิลฟีนอกซีฟอสฟิน-โพลีเอทิลีนไกลคอลที่มีโลหะอัลคาไลน์ ซึ่งสามารถนำข้อมูลที่ได้ไปใช้ออกแบบและพัฒนาตัวเร่งปฏิกิริยาต่อไป

สาขาวิชา เคมี
ปีการศึกษา 2564

ลายมือชื่อนิสิต
ลายมือชื่อ อ.ที่ปรึกษาหลัก

6072811123 : MAJOR CHEMISTRY

KEYWORD: Phenoxy-imine (FI) catalysts, Nickel phenoxyphosphine-polyethylene glycol (Ni-PEG) catalysts, Ethylene polymerization, DFT calculations, Reaction mechanism

Pavee Apilardmongkol : THEORETICAL STUDY OF ETHYLENE POLYMERIZATION BY PHENOXY-IMINE CATALYSTS. Advisor: Prof. VUDHICHAJ PARASUK, Ph.D.

Reaction mechanisms of ethylene polymerization catalyzed by the phenoxy-imine (FI) and the nickel phenoxyphosphine polyethylene glycol (Ni-PEG) with alkali metals were explored using DFT calculations. For FI catalysts, the effect of group IV_B transition metals substitutions was investigated. The trend of calculated activation energies (E_a) at the rate-determining step is Zr < Hf < Ti and is in good agreement with experiments. The effect of ligands of the Ti-FI-based catalysts when changing the parent nitrogen (O, N) to oxygen (O, O), phosphorus (O, P), and sulfur (O, S) ligands on activity was also monitored. The results indicated that the sulfur (O, S) ligand gives the lowest activation energy. Additionally, the reactivity of Ni-phenoxy-imine (Ni-FI)-based catalysts for polyethylene polymerization was studied. Our calculations suggested that the square planar complex of Ni-FI is more reactive than its C₂ symmetric octahedral complex. For Ni-PEG(M) catalysts, the trend for activation energies of four Ni-PEG(M) systems is Li < Na < K < Cs, which corresponds to experimentally observed activities. Moreover, the roles of secondary metals in Ni-PEG catalysts in terms of steric, electronic, and electrostatic effects were elucidated. The DFT results suggested that the active catalyst should have strong cooperative metal-metal/metal-ligand interactions and less positive charge on the secondary metal. Finally, to gain insight into the design of the novel Ni-PEG catalysts with alkali-earth metals, the effect of catalyst structure on experimental activity was investigated. This work provides fundamental understandings of the reaction mechanisms for the FI and Ni-PEG(M) catalysts, which could be used for the design and development of catalysts for ethylene polymerization.

Field of Study: Chemistry

Student's Signature

Academic Year: 2021

Advisor's Signature

ACKNOWLEDGEMENTS

The thesis for a Doctor of Philosophy degree could not have been completed without the good instruction, encouragement, and support throughout five years of study at Chulalongkorn University.

I would like to thank my advisor, Prof. Vudhichai Parasuk, for giving useful guidance, conceptualizing the research and revision during the time of my research. I also thank all the members of the VP group for their help.

I would like to thank my thesis committee, Asst. Prof. Dr. Varawut Tangpasuthadol, Assoc. Prof. Dr. Somsak Pianwanit, Dr. Junjuda Unruangsri, and Dr. Chompoonut Rungnim for giving several suggestions. In addition, I would also like to thank Prof. Jun-ya Hasegawa and Dr. Manussada Ratanasak for giving useful suggestions and collaborating on my publications. A special thanks for the great opportunity to do long-term research at Hokkaido University.

For this, I would like to thank the financial support from the Development and Promotion of Science and Technology Talents Project (DPST). I would like to express my gratitude to the Center of Excellence in Computational Chemistry (CECC), the National e-Science Infrastructure Consortium and the Institute for Catalysis (ICAT) at Hokkaido University for providing high-performance computing services and facilities.

Finally, I would like to express my thanks to my family and my friends for all their support and encouragement. Without these people, this dissertation wouldn't be successful or possible.

Pavee Apilardmongkol

TABLE OF CONTENTS

	Page
ABSTRACT (THAI)	iii
ABSTRACT (ENGLISH)	iv
ACKNOWLEDGEMENTS	v
TABLE OF CONTENTS	vi
LIST OF FIGURES	1
LIST OF TABLES	4
CHAPTER I INTRODUCTION.....	5
1.1 Research rationale.....	5
1.2 Catalysts for ethylene polymerization.....	6
1.2.1 Ziegler-Natta catalysts	6
1.2.2 Metallocene catalysts.....	7
1.2.3 Post-metallocene catalysts	8
1.2.3.1 Phenoxy-imine (FI) catalysts.....	8
1.2.3.2 Nickel phenoxyphosphine polyethylene glycol (Ni-PEG) catalysts.	9
1.3 Mechanism of ethylene polymerization	10
1.3.1 FI catalysts.....	11
1.3.2 Ni-PEG catalysts.....	11
1.4 Literature reviews.....	13
1.5 Scope of this research.....	15
CHAPTER II THEORY BACKGROUND	17
2.1 Quantum mechanics	17

2.1.1 The Schrödinger equation.....	17
2.1.2 The Born-Oppenheimer approximation	18
2.1.3 The Hartree-Fock method.....	19
2.2 Density Functional Theory (DFT).....	20
2.2.1 Hohenberg-Kohn theorem and Kohn-Sham equation	20
2.2.2 Exchange correlation functional	22
2.2.3 Basis set	23
CHAPTER III CALCULATION DETAILS	24
3.1 FI catalysts	24
3.1.1 Computational models.....	24
3.1.2 DFT calculations.....	25
3.2 Ni-PEG catalysts	27
3.2.1 Computational models.....	27
3.2.2 DFT calculations.....	28
CHAPTER IV RESULTS AND DISCUSSION	30
4.1 FI catalysts	30
4.1.1 Stability of pre-reaction complexes.....	30
4.1.2 Effect of metal substitutions	31
4.1.3 Effect of ligand substitutions.....	35
4.1.4 Novel Ni-phenoxy-imine (Ni-FI) catalysts with (O, N) ligand.....	37
4.2 Ni-PEG catalysts	38
4.2.1 Reaction pathways of Ni-PEG(M) for ethylene polymerization	39
4.2.2 Influence of catalyst structures on experimental activity.....	43
CHAPTER V CONCLUSIONS.....	47

REFERENCES 49

VITA..... 57



จุฬาลงกรณ์มหาวิทยาลัย
CHULALONGKORN UNIVERSITY

LIST OF FIGURES

	Pages
Figure 1 Component of the Ziegler-Natta catalyst for olefin polymerization.	7
Figure 2 Activation of the metallocene catalyst for olefin polymerization [14].	7
Figure 3 Examples of metallocene, half-metallocene, and post-metallocene catalysts for olefin polymerization [15].	8
Figure 4 The pre-reaction structure of FI catalysts.	9
Figure 5 Active species of FI complexes after being activated with MAO or borate as cocatalyst systems [19].	9
Figure 6 The pre-reaction structure of Ni-PEG catalysts.	10
Figure 7 The proposed mechanism for ethylene polymerization is based on the Cossee-Arlman mechanism, the Green-Rooney mechanism, and the transition-state α -agostic mechanism [24].	10
Figure 8 Reaction mechanism of ethylene polymerization catalyzed by phenoxy-imine (FI) catalysts.	11
Figure 9 Reaction mechanism for ethylene polymerization catalyzed by Ni-PEG with alkali metals (M).	13
Figure 10 Examples of highly active ethylene polymerization catalysts [17].	14
Figure 11 Density functional theory (DFT) neglects the many particles electron in term of electron density [38].	20
Figure 12 Flow chart for solving the Kohn-Sham equation [43].	22
Figure 13 The FI catalyst's molecular structure for the pre-reaction complex (left) and the reactant π -complex (right). Where M is group IV _B transition metals (Ti, Zr, Hf).	25
Figure 14 Heterobimetallic Ni-PEG with alkali metals (M = Li, Na, K, and Cs) for pre-reaction model (left) and for reaction pathway model (ethylene insertion complex,	

right). The geometric isomers A (top) and B (bottom) were defined. R = CH₃ and R = C₃H₇ as a growing chain for the first and second ethylene insertions, respectively. ... 27

Figure 15 The relative potential energy (RE) in kcal mol⁻¹ of the five possible isomers (A-E) at the pre-reaction Ti-FI states. Isomer A is the most stable and is the reference. 31

Figure 16 Relative potential energy profiles of ethylene polymerization by the FI catalysts. Different groups of IV_B (Ti, Zr, Hf) transition metals were compared. The potential energies relative to R₁ are given in kcal mol⁻¹. 32

Figure 17 Relative energy profiles for ethylene polymerization catalyzed by (Ti-1)-FI catalyst in the gas phase (blue line) and toluene (red line). The energies relative to R₁ are given in kcal mol⁻¹. The relative Gibbs free energy (ΔG^\ddagger) at 298.15 K is shown in parenthesis. 32

Figure 18 The molecular electrostatic potential (MEP) maps and NBO charges of (a) (Ti-1)-FI (b) (Zr-1)-FI (c) (Hf-1)-FI of the reactant π -complex (R₂). The isosurface value is 0.002, with a range for the MEPs map of 0.06 to 0.12 a.u. 34

Figure 19 Optimized TS structures of Ti-1 with (a) (O, N) (b) (O, P) (c) (O, O) (d) (O, S) ligands and Ti-3 with (e) (O, N) (f) (O, S) ligands. The carbon, hydrogen, oxygen, nitrogen, phosphorus, sulfur, and titanium atoms are shown in grey, white, red, blue, orange, yellow, and light pink, respectively. The ethylene (ET) molecule is shown in a dark pink. Distances (Å) are given in blue and red. 36

Figure 20 Optimized structures of the reactant π -complex (R), transition state (TS), and β -agostic product (P) for the ethylene polymerization catalyzed by (a) octahedral Ni-FI and (b) square planar of half Ni-FI. Bond distances (Å) are displayed in blue and red. 38

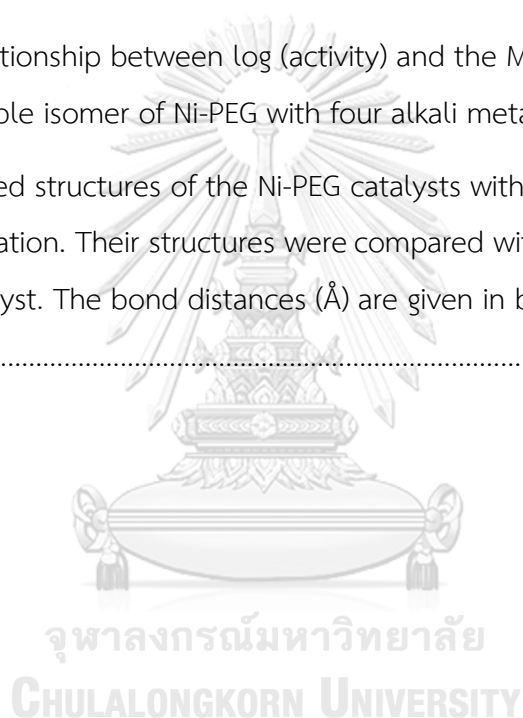
Figure 21 Relative potential energy profiles for ethylene polymerization catalyzed by Ni-PEG. Favorable pathways for alkali metals (M = Li, Na, K, and Cs) were compared. The potential energies relative to the complex R_A are given in kcal mol⁻¹. 39

Figure 22 Optimized structure of the reactant (R_A) and transition state (TS_B) for ethylene polymerization by Ni-PEG catalysts with different alkali metals (M) (a) Li (b) Na (c) K, and (d) Cs for the first ethylene insertion ($R = CH_3$) of the favorable pathway. The H atoms were omitted for clarity..... 41

Figure 23 Optimized structure of transition state (TS_B) for ethylene polymerization by Ni-PEG catalysts with different alkali metals for the first ethylene insertion ($R = CH_3$) of the favorable pathway. Distances (\AA) are given in blue, and NBO charges are shown in black. 42

Figure 24 The relationship between $\log(\text{activity})$ and the $M-O_1$ and $M-O_{PEG}$ distances from the most stable isomer of Ni-PEG with four alkali metals (M cation)..... 45

Figure 25 Optimized structures of the Ni-PEG catalysts with (a) Be (b) Mg (c) Ca (d) Sr (e) Co and (f) Zn cation. Their structures were compared with that of the most active (g) Ni-PEG (Li) catalyst. The bond distances (\AA) are given in blue. The H atoms are omitted for clarity..... 46



LIST OF TABLES

Pages

Table 1 Comparison of bond distances (Å) and bond angles (°) of the pre-reaction complex (Ti-1) between X-ray structure [18] and seven theoretical methods with the cc-pVDZ basis set.	26
Table 2 Bond lengths (Å), bond angles (°), dihedral angles (°) of isomer A's optimized Ni-PEG(Li) structure with different method/basis set.	29
Table 3 Experimental activities and our DFT calculation results. The energies are given in kcal mol ⁻¹	33
Table 4 The calculated activation energy (E_a^{RDS}) and reaction energy (ΔE_r^{RDS}) of different ligand substitutions of Ti-1 (O, X) and Ti-3 (O, X) systems at the rate-determining step.	35
Table 5 Selected bond lengths (Å), bond angles (°), dihedral angles (°), and NBO charges of Ni-PEG. When M = Li, Na, K, and Cs.	44

CHAPTER I

INTRODUCTION

1.1 Research rationale

Polyethylene (PE) is an integral part of our daily life, for instance, plastic shopping bags, food packages, shampoo and detergent bottles, containers, storage boxes, toys, disposable diapers, sneakers, etc. [1]. PE is produced either by the addition or radical polymerization of ethylene monomers. Commercially, Ziegler-Natta and metallocene catalysts have been employed for the polymerization of polyethylene. However, these catalysts are not perfect because of the existing of multiple active sites in their structures. Therefore, the development of single-site metallocene catalysts attracts the polyolefin industry. Phenoxy-imine (FI) catalysts, one type of post-metallocene catalyst, have been introduced for olefin polymerization [2]. They are composed of group IVB transition metal complexes with two phenoxy-imine ligands. Many studies report that FI catalysts show high activity for ethylene polymerization when activated with methylaluminoxane (MAO). Moreover, several experimental and computational studies have been performed to understand and improve catalytic activities. The highly active catalyst should provide low activation energy [3]. Nevertheless, there are few studies that address the reaction mechanism of these catalysts. Thus, it is in our interest to perform DFT calculations on mechanistic features to gain insight into the ethylene polymerization catalyzed by FI catalysts.

Recently, heterobimetallic catalysts that contain two different metals in a single platform have been found to significantly improve the catalytic reactivity [4]. The heterobimetallic catalysts can enhance polymerization reactivity with multiple explicit interactions. The use of two different metals possibly affects the olefin insertion and increases or decreases the rate of polymerization. The advantage of heterobimetallic complexes is the significant improvement of the catalytic activity

when compared to monometallic catalysts [5]. The late transition metal catalysts containing nickel with phenoxyphosphine ligand and polyethylene glycol were introduced as excellent catalysts for ethylene polymerization [6]. However, no studies on the catalysts' reaction mechanisms have been conducted. Hence, the ethylene polymerization catalyzed by nickel phenoxyphosphine polyethylene glycol (Ni-PEG) catalysts with different alkali metals (M) was additionally investigated. The key factors of Ni-PEG (M) catalysts were elucidated to provide a further design for Ni-PEG (M) catalysts. The knowledge obtained in this study will lead to the development of a more active catalyst for ethylene polymerization.

1.2 Catalysts for ethylene polymerization

1.2.1 Ziegler-Natta catalysts

Since Karl Ziegler and Giulio Natta were awarded the Nobel Prize during the early 1950s, in 2015, polyolefin materials such as polyethylene (PE) and polypropylene (PP) were accounted for nearly half of the 300 million tons of global plastics production [7]. Several industrially relevant thermoplastic materials (polyethylene, isotactic polypropylene) and rubbers (polybutadiene, polyisoprene, and ethene-propene copolymers) are produced with Ziegler-Natta catalysts [8]. The Ziegler-Natta catalyst mainly consists of four components: $MgCl_2$ as catalyst support, $TiCl_4$ as the active catalyst precursor, AlR_3 (R = alkyl group) as a catalyst activator, and the Lewis base [9], **Figure 1**. Many modern Ziegler-Natta catalysts have several advantages. They produce high molecular weight polymers, exhibit high activity and better control morphology [10]. However, the disadvantages of Ziegler-Natta catalysts are that they have less control of the growing polymer chain because of the multiple active sites of transition metals, the encapsulation effect of polymer chains, and the difficulty of removing the catalyst from the final product [11].

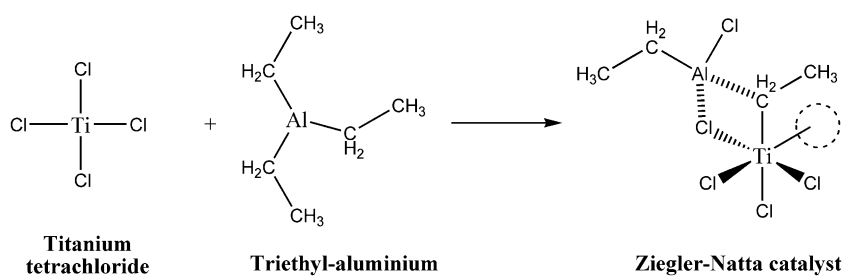


Figure 1 Component of the Ziegler-Natta catalyst for olefin polymerization.

1.2.2 Metallocene catalysts

Single-site metallocene catalysts have the ability to produce polymers with controlled molecular weight, improved molecular weight distribution, specific tacticity, and better co-monomer distribution and content [12]. General metallocene catalysts are composed of transition metals sandwiched between two cyclopentadienyl rings. Methylaluminoxane (MAO) plays a crucial part in generating a vacant site for ethylene insertion of the metallocene catalyst [13]. The activation process of the metallocene catalyst is shown in **Figure 2**.

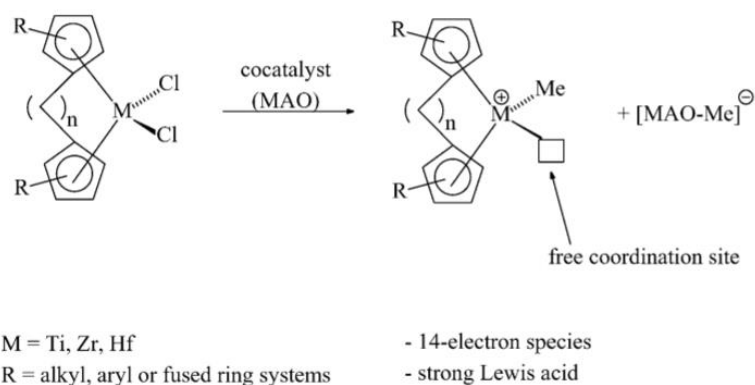


Figure 2 Activation of the metallocene catalyst for olefin polymerization [14].

The single-site metallocene catalysts have been developed into several designs. By substitution of one Cp ring to other components, the catalysts are called half-metallocene, and by completely substituting other ligands, they are called post-metallocene, as shown in **Figure 3**.

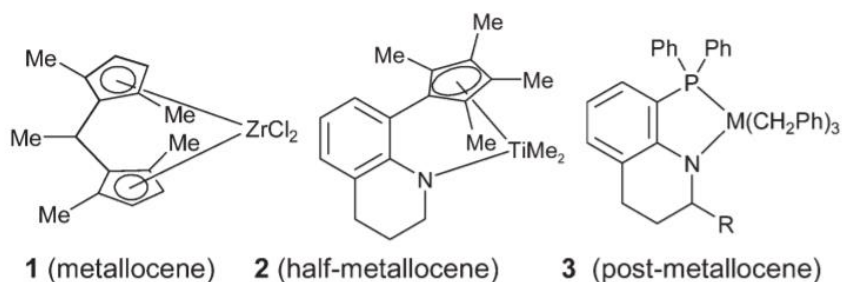


Figure 3 Examples of metallocene, half-metallocene, and post-metallocene catalysts for olefin polymerization [15].

1.2.3 Post-metallocene catalysts

In the last two decades, post-metallocene or non-metallocene catalysts have been commercialized for the polymerization industry [16]. Based on the “ligand-oriented catalyst design concept,” which believes that the flexible electronic nature of ligands may possibly enhance catalytic activity [17], the development of post-metallocene catalysts becomes attractive.

1.2.3.1 Phenoxy-imine (FI) catalysts

Phenoxy-imine (FI) catalysts, one type of post-metallocene catalyst, are composed of transition metals connected to phenoxy-imine (O, N) ligands in octahedral geometry. The pre-reaction structure in which the metal (M) center connects to two imine nitrogens, two phenolic oxygens, and two chloro ligands is shown in **Figure 4**. Previous DFT calculations revealed that the structure with *cis-N/trans-O/cis-Cl* is the most stable isomer [18]. Several studies have reported that FI catalysts have high ethylene polymerization activity when activated with methylaluminoxane (MAO) (see **Figure 5**) [2, 19]. However, there are few studies that addressed the mechanism of ethylene polymerization catalyzed by FI. The ethylene polymerization activity of FI catalysts with different metals was reported by Mitani et al. [19]. The highest activity was obtained with Zr-FI, followed by Hf-FI and Ti-FI catalysts, respectively.

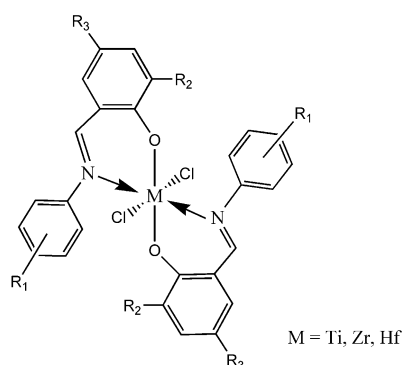


Figure 4 The pre-reaction structure of FI catalysts.

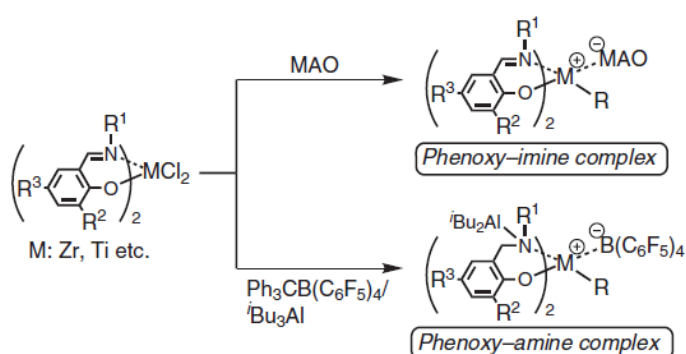


Figure 5 Active species of FI complexes after being activated with MAO or borate as cocatalyst systems [19].

1.2.3.2 Nickel phenoxyphosphine polyethylene glycol (Ni-PEG) catalysts

Several heterobimetallic catalysts have been introduced for olefin polymerization [20, 21]. Heterobimetallic catalysts have two different metals on a single platform, which differs from homobimetallic and monometallic. The presence of secondary metal could effectively accelerate the ethylene polymerization rate of nickel phenoxyphosphine catalysts [4]. In this work, we focused on the nickel phenoxyphosphine polyethylene glycol (Ni-PEG) with different alkali metals (Li, Na, K, and Cs). Experimental results reported that the Ni-PEG with Li as a secondary metal provided the highest activity at moderate temperatures, followed by Na, K, and Cs, respectively [22]. **Figure 6** depicts the pre-reaction structure of Ni-PEG catalysts, which

consists of a nickel metal center, phenoxyphosphine ligand, trimethyl-phosphine, phenyl, polyethylene glycol, and alkali metal (M = Li, Na, K, and Cs).

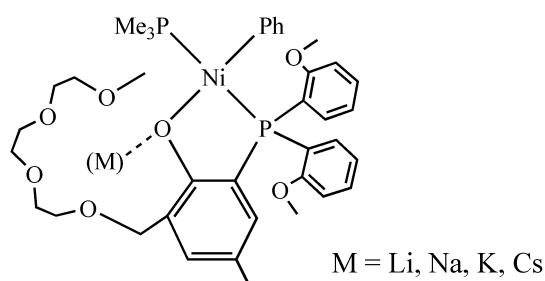


Figure 6 The pre-reaction structure of Ni-PEG catalysts.

1.3 Mechanism of ethylene polymerization

Ethylene polymerization mechanisms exhibit several features that differ from other polymerization [23]. The idea for the proposed mechanism of ethylene polymerization is based on the Cossee–Arlman mechanism, the Green–Rooney mechanism, and the transition-state α -agostic mechanism, which are shown in **Figure 7**.

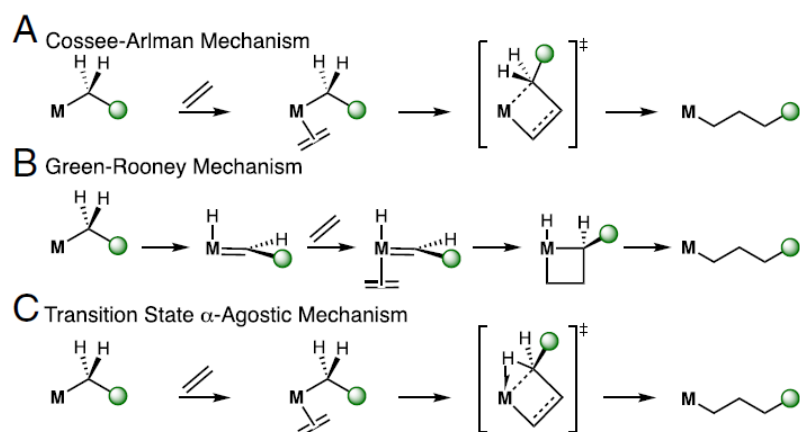


Figure 7 The proposed mechanism for ethylene polymerization is based on the Cossee–Arlman mechanism, the Green–Rooney mechanism, and the transition-state α -agostic mechanism [24].

1.3.1 FI catalysts

Based on the Cossee-Arlman mechanism, the mechanism of ET polymerization by FI catalyst was originally suggested by Nikitin et al. [25]. As depicted in **Figure 8**, the reactant π -complex (R_1) was selected as a starting structure for the reaction mechanism. Then, the first ethylene was inserted into the transition metal-alkyl bond via a four-membered ring transition state (TS_1) and generated the β -agostic product (P_1). The structure was then rearranged to form the active complex (A_2) via a five-coordinated ethylene insertion. The reaction continued with a new ethylene monomer inserted into transition metal, which is similar to the first ethylene insertion. For the second ethylene insertion, the reaction continues with the reactant π -complex (R_2), the four-membered ring transition state (TS_2), and the β -agostic product (P_2).

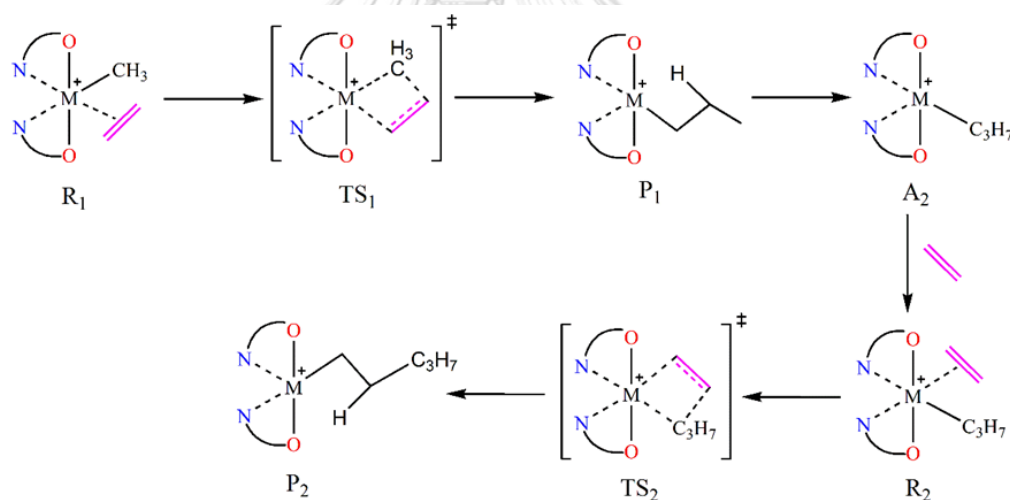


Figure 8 Reaction mechanism of ethylene polymerization catalyzed by phenoxy-imine (FI) catalysts.

1.3.2 Ni-PEG catalysts

The proposed reaction mechanism for ethylene polymerization catalyzed by Ni-PEG with alkali metal (M) was depicted in **Figure 9**. The mechanism is based on Tran et al. [22], which suggested the *cis-to-trans* isomerization of the reactant state as the key step. The reactant π -complex (R) was selected as a starting structure to elucidate the reaction mechanisms. The subscripts A (ethylene *cis* to oxygen) and B (ethylene

trans to oxygen) represent the position of ethylene insertion into the nickel-metal center. The ethylene insertion *cis* to oxygen is favored over its isomer. Therefore, the favorable pathway begins with the most stable reactant π -complex (R_A), which proceeds via a pentacoordinate transition state of isomerization (TS_{iso}) step to obtain a less stable reactant π -complex (R_B). Then, the first ethylene inserted into the Ni-alkyl bond via the four-membered-ring transition state (TS_B) and generated the stable β -agostic product (P_B). Then, the second ethylene monomer is inserted together with the β -hydrogen elimination (TS_{BA}) into the Ni-metal center to form the stable reactant π -complex (R_{A2}). On the other hand, the P_B structure can be rearranged to generate a vacant site complex (V_{BA}) via an unstable tri-coordinated complex for the second ethylene insertion. The subscript BA means the connection between the stable β -agostic product (P_B) of the first ethylene insertion and the reactant π -complex (R_{A2}) of the new ethylene monomer. For the second ethylene insertion, the isomerization proceeds like the first insertion, which is followed by a transition state of isomerization (TS_{iso2}), a reactant π -complex (R_{B2}), a transition state (TS_{B2}), and the β -agostic product (P_{B2}) of the second insertion.

Another possible path, which is the kinetically unfavorable pathway, is where R_A is converted into the β -agostic product (P_A) via the four-membered ring transition state (TS_A). Then, the structure is rearranged to generate a vacant site complex (V_{AB}). The subscript AB means the process from the β -agostic product (P_A) of the first ethylene insertion to obtain the reactant π -complex (R_{B2}) of the second insertion. In addition, the R_{A2} also undergoes the transition state (TS_{A2}) and reaches the β -agostic product (P_{A2}), like the first ethylene insertion.

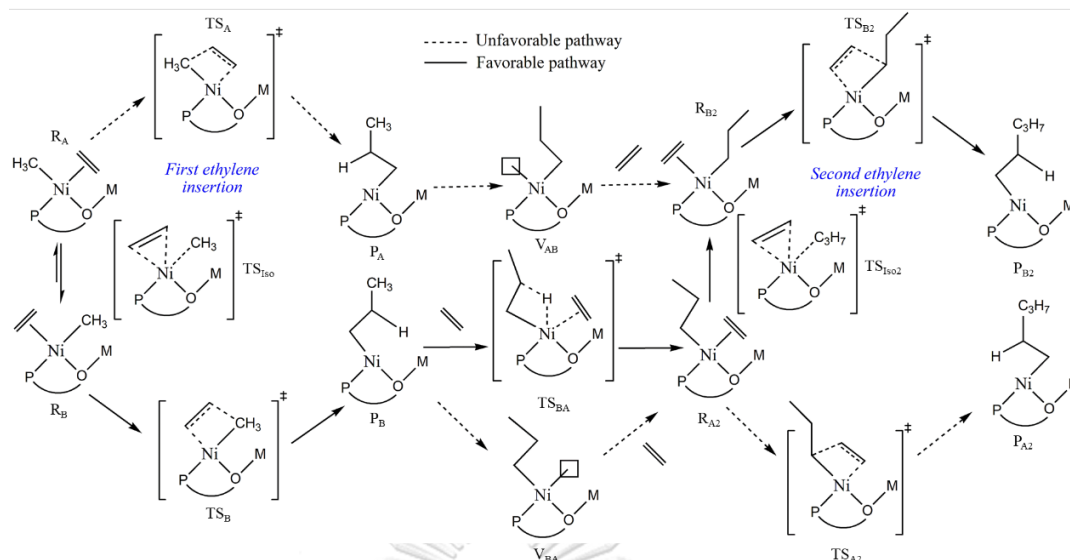


Figure 9 Reaction mechanism for ethylene polymerization catalyzed by Ni-PEG with alkali metals (M).

1.4 Literature reviews

In 2002, Makio et al. [18] first introduced the FI catalyst and investigated its macroscopic properties and catalytic behavior. The catalyst name FI comes from the Japanese pronunciation of the ligand “Fenokishi-Imin”. They found that the octahedral dichloride of the FI complex having *cis-N/trans-O/cis-Cl* is the most stable one among five possible isomers. The X-ray structures of the Ti-FI and Zr-FI complexes were reported. Moreover, the Zr-FI displayed very high ethylene polymerization activity under mild conditions.

In 2004, Mitani et al. [19] reported the catalytic activities of FI catalysts with different transition metals. Under mild conditions, the Zr-FI exhibited the highest activity, followed by the Hf-FI and Ti-FI.

In 2008, Matsugi and Fujita [17] introduced the designed concept for olefin polymerization. Using FI ligated with transition metals provided a highly active catalyst for ethylene polymerization when compared with others, for instance, pyrrolide-imine (PI catalyst), indolide-imine (II catalyst), phenoxy-ether (FE catalyst), imine-phenoxy (IF catalyst), phenoxy-pyridine (FP catalyst), which are shown in **Figure 10**.

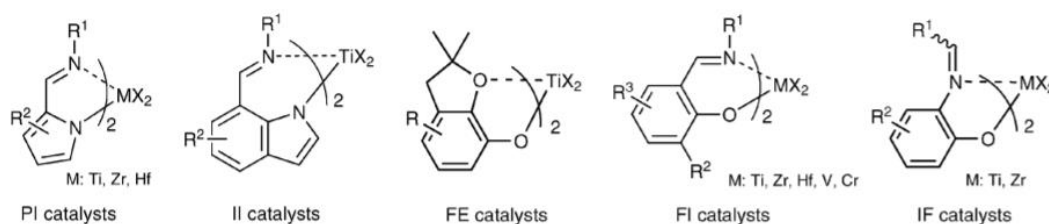


Figure 10 Examples of highly active ethylene polymerization catalysts [17].

In 2011, Terao et al. [26] studied the significant substituent effects on the activity of FI catalysts. They summarized that an increase in the steric bulkiness of the substituent can enhance the catalytic activity.

In 2015, Damavandi et al. [27] introduced the Ni complexes with naphtholato imine group ligands that were designed, synthesized, and characterized. However, the catalyst displayed moderate ethylene polymerization activity.

In 2016, Nikitin et al. [25] conducted a study that describes the mechanism of ethylene polymerization on Ti-FI catalysts to identify the major factors affecting the catalytic activities. They performed DFT calculations using the BP86 exchange-correlation functional and the SVP split-valence basis set for all atoms. The proposed mechanism has four stages: pre-reaction, activation, propagation, and termination. They found that the propagation reaction has a strong influence on the activity of the catalysts. The electronic and steric effects of the ligand control the total catalytic activity. The major factor affecting the catalytic activity depends on the structure of the active site. Theoretical and experimental data on FI catalysts with different substitutions as well as activity values were reported. The substitution of tert-butyl (in the R_2 position of **Figure 4**) with an allyloxy group (OAll) in the para position of the N-aryl moiety (R_1 position of **Figure 4**) resulted in the highest Ti-FI activity. In addition, their results suggest that HOMO-LUMO gaps in the active cations can affect the catalytic activities.

In 2018, Chasing et al. [28] performed quantitative structure-activity relationship (QSAR) studies of the Ti-FI series to illustrate the structural properties of FI catalysts

related to the polymerization activity. The new design of the FI catalyst with Ni was proposed as a candidate catalyst for polyethylene polymerization.

In 2019, Tran and co-workers [6] first designed a new class of heterobimetallic nickel-sodium phenoxyphosphine polyethylene glycol called Ni-PEG (Na). They discovered that the presence of sodium cations can affect the rate of polymerization. The polyethylene glycol (PEG) group was enriched with nickel cations or alkali metal cations. Four ether oxygens of the PEG group provide metal binding sites for cations which control the architecture of the polymer during ethylene polymerization [29]. As a result, the existence of secondary metals could significantly improve the catalytic activity. Moreover, the influence of the PEG unit was able to enhance catalytic activity, catalytic stability, and molecular weight [30].

In 2020, Tran et al. [22] investigated the effects of secondary metals (M) on Ni-PEG catalysts and illustrated that Ni-PEG exhibited higher activity than monometallic nickel catalysts because the metal-PEG group prevented interaction at the axial position of nickel. The Ni-PEG with Li as a secondary metal provided the highest activity, followed by Na, K, and Cs at moderate temperatures (30-50 °C). Differences in the secondary metal sizes are possibly controlled and boost catalytic performance. Consequently, the platform of phenoxyphosphine ligands connected to the PEG group could easily be designed to accommodate several secondary metals.

1.5 Scope of this research

We performed density functional theory (DFT) calculations to elucidate the mechanism of ethylene polymerization catalyzed by FI catalysts. The relative stability of five possible isomers of pre-reaction Ti-FI dichloride complexes was first determined to select the most stable isomer. Then, the potential energy profiles of the active form FI catalysts were calculated and employed to gain insight into the reaction mechanism of FI catalysts with different groups of IV_B transition metals (M = Ti, Zr, Hf) substitutions. Both activation energies and structural properties were mainly compared to catalytic activities. The effects of ligand substitutions were investigated by changing the parent

nitrogen (O, N) into oxygen (O, O), phosphorus (O, P) and sulfur (O, S) ligands. After that, we examined novel Ni-FI based catalysts to provide candidate catalysts for ethylene polymerization.

On the other hand, the reaction mechanism of ethylene polymerization catalyzed by Ni-PEG with different alkali metals was investigated. Both steric and electronic effects on the activation energy were investigated. Finally, the influence of pre-reaction structure on experimental activities was analyzed to design more active catalysts for ethylene polymerization.



CHAPTER II

THEORY BACKGROUND

2.1 Quantum mechanics

Quantum mechanics (QM) has been developed over a century to describe microscopic phenomena. QM is the fundamental theory of physics that describes the physical properties of matter with energy at the atomic scale and subatomic particles. Quantum mechanics is merged with many other areas of modern science. Thus, understanding the main ideas and methods of quantum mechanics is important for developing many branches of science, from nuclear physics to organic chemistry [31].

2.1.1 The Schrödinger equation

The Schrödinger equation is basically a differential equation and is widely used in chemistry and physics to solve problems relating to quantum materials. The Schrödinger wave equation describes the behavior of a particle in terms of force or the change of a physical quantity over time. Schrödinger, who developed the equation, was even awarded the Nobel Prize in 1933 for the discovery of new productive forms of atomic theory. The Schrödinger wave equation is a mathematical expression based on three considerations, which are the classical plane wave equation, De Broglie's hypothesis of matter-wave, and conservation of energy [32].

The general form of the time-dependent Schrödinger equation, which is used to find the wave function depends on time, is represented as;

$$i\hbar \frac{d}{dt} |\Psi(t)\rangle = \hat{H} |\Psi(t)\rangle \quad (2.1)$$

$$i\hbar \frac{\partial}{\partial t} \Psi(\vec{r}, t) = \left[-\frac{\hbar^2}{2m} \nabla^2 + V(\vec{r}, t) \right] \Psi(\vec{r}, t) \quad (2.2)$$

where i is imaginary unit, Ψ is the time-dependent wavefunction, \hat{H} is the Hamiltonian operator, \hbar is the reduced Planck constant, and $V(\vec{r}, t)$ is the potential that represents the environment in which the particle exists with the spatial coordinates (\vec{r}) at time (t) .

The time-independent Schrödinger equation, which is used to find the wavefunction from the stationary state, can be expressed as;

$$\hat{H}\Psi = E\Psi \quad (2.3)$$

where E is the energy of the system, \hat{H} is the Hamiltonian operator, and Ψ is the time-independent wave function.

The Schrödinger equation plays the role of Newton's laws and conservation of energy in classical mechanics to describe the behavior of a system in terms of a wave function. The combination of kinetic and potential operators, so called the Hamiltonian operator, acts upon the wave function. The Schrödinger equation gives the quantized energies of the system. Moreover, several properties can be elucidated from the wave function. However, this equation can be solved exactly for one electron system, for example, hydrogen atoms and hydrogen-like ions (He^+ , Li^{2+} , Be^{3+} , and B^{4+}). Because the Coulomb interactions between the electrons can be solved just difficult.

2.1.2 The Born-Oppenheimer approximation

The Born-Oppenheimer approximation is the assumption that the nuclear motion and electronic motion in molecules can be separated. Generally, the electronic wave function can be determined as the electron positions and nuclear positions. However, the electronic wavefunction depends on positions but does not include their velocities. For example, nuclear motion is much slower than electron motion. Thus, the Born-Oppenheimer approximation can neglect the motion of the atomic nuclei when determining the electrons in a molecule. The Hamiltonian operator can be split into two or more terms and can reduce the problem in which it is influenced by the motion of the nucleus [33]. Thus, the time-independent Schrödinger equation for molecular systems can be expressed as:

$$\left[-\frac{1}{2} \sum_i \nabla_i^2 - \sum_A \frac{1}{2M_A} \nabla_A^2 - \sum_{A,i} \frac{Z_A}{r_{Ai}} + \sum_{A>B} \frac{Z_A Z_B}{R_{AB}} + \sum_{i>j} \frac{1}{r_{ij}} \right] \Psi(\mathbf{r}, \mathbf{R}) = E_{elec} \Psi(\mathbf{r}, \mathbf{R}) \quad (2.4)$$

$$[T_e + T_N + V_{eN} + V_{NN}(\mathbf{R}) + V_{ee}(\mathbf{r})] \Psi(\mathbf{r}, \mathbf{R}) = E_{elec} \Psi(\mathbf{r}, \mathbf{R}) \quad (2.5)$$

where i, j refer to the electrons (e), A, B refer to the nucleus (N), Z is the nuclear charge, M_A is the mass of nucleus A , R is the distance between the nucleus, r_{Ai} is the distance between nucleus A and electron i , r_{ij} is the distance between electron i and j , T_e is the kinetic energy of electrons, T_N is the kinetic energy of the nucleus, and V_{eN} , V_{NN} , and V_{ee} are the Coulomb repulsion.

The electronic wave function, which contains lots of useful information about molecular properties such as dipole moments, polarizability, etc.

2.1.3 The Hartree-Fock method

The Hartree-Fock method was developed to solve the time-independent Schrödinger equation for the system which contains electrons and nuclei [34]. The Hartree-Fock method assumes that the wavefunction can be approximated by single Slater determinant of the set of orbitals which can be obtained through variation principle. The Hartree-Fock equation can be expressed as:

$$f(\mathbf{x}_1) \chi_i(\mathbf{x}_1) = \varepsilon_i \chi_i(\mathbf{x}_1) \quad (2.6)$$

$$f(\mathbf{x}_1) = h(\mathbf{x}_1) + \sum_j J_j(\mathbf{x}_1) - K_j(\mathbf{x}_1) \quad (2.7)$$

where ε_i is the energy associated with orbital χ_i , $h(\mathbf{x}_1)$ is the one-electron operator $J_j(\mathbf{x}_1)$ is the Coulomb operator, and $K_j(\mathbf{x}_1)$ is an exchange operator. Thus, the equation (2.6) is pseudo-eigen valued equation and its solution can be obtained using method of self-consistent field (SCF).

The Coulomb operator gives the Coulomb interaction of an electron in a spin orbital (x_i) with the average charge distribution of the other electrons. The exchange operator gives exchanges spin orbitals x_i and x_j .

By the introduction of basis set, the Hartree-Fock equations can be transformed into the Roothaan-Hall equations, which are expressed as:

$$\mathbf{FC} = \mathbf{SC}\boldsymbol{\varepsilon} \quad (2.8)$$

where F is the Fock matrix, C is the matrix of molecular orbital coefficients, S is the overlap matrix of the basis functions, and $\boldsymbol{\varepsilon}$ is the matrix of orbital energies.

2.2 Density Functional Theory (DFT)

DFT is a quantum mechanical method used to investigate the electronic structure of many-body systems [35]. The DFT provides low computational cost and high accuracy, which makes the DFT technique applicable in most branches of chemistry and materials science [36]. The basic idea is that the electron density at each point determines the ground-state properties of an atomic or molecular system [37]. The many-body perspective depends on all the spatial coordinates of all electrons in the system, while the electron density is computationally determined as a simple object (see **Figure 11**).

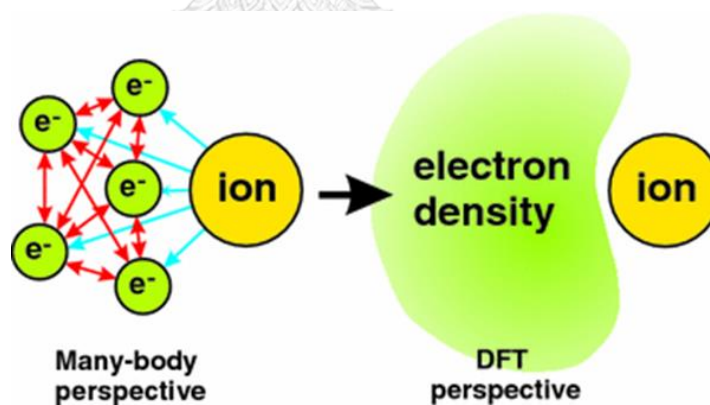


Figure 11 Density functional theory (DFT) neglects the many particles electron in term of electron density [38].

2.2.1 Hohenberg-Kohn theorem and Kohn-Sham equation

The basic foundation of DFT is the Hohenberg-Kohn theorem, which relates to any system consisting of electron motion under the influence of an external potential [39]. The first Hohenberg-Kohn theorem states that the ground state of interacting

many-particle systems is a unique functional of the electron density. The second Hohenberg–Kohn theorem states that the ground state energy of the system is obtained via minimization of the energy functional with respect to the electron density [40]. However, this theory does not offer a way to compute the ground-state density of a system in practice. The Kohn–Sham (KS) theory is formulated as a simple expression of the ground state energy [41]. Solutions of the Kohn–Sham equation can be used to describe the electronic structure of several nanostructures, such as nanowires, nanotubes, or quantum dots [42]. **Figure 12** displays the flow chart of solving the KS equation starting from defining an initial/trial electron density. An approximation of the potential energy was obtained by solving the Kohn–Sham equations to find the single-particle wave function. The electron density is defined by the Kohn–Sham single particle wave function. Then, the calculated electron density is evaluated. If the calculated electron density and the electron density used in solving the Kohn–Sham equations are the same, this is referred to as the “ground-state electron density” and can be used to compute the total energy. If these two electron densities were different, the trial electron density would be updated in some way.

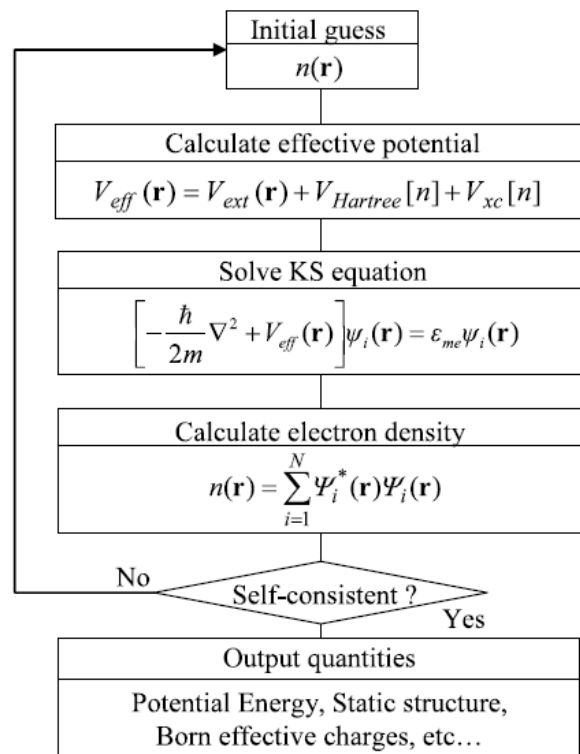


Figure 12 Flow chart for solving the Kohn-Sham equation [43].

2.2.2 Exchange correlation functional

The construction of the exchange correlation functional plays an important role in calculating the functional of the electron density. The exchange correlation functional is a part of the approximation in the Kohn-Sham equation. The exchange correlation energy accounts for the remaining electronic energy not included in the non-interacting kinetic and electrostatic terms. In modern exchange correlation functionals, the electronic energy depends on several properties or functionals of the electron density, local and nonlocal [44]. The reliability of the method depends on the validity of the approximated functional. The exchange-correlation functionals are classified based on their characteristics, which are composed of:

- Local density approximation (LDA): functionals of only electron density
- Generalized gradient approximation (GGA): functionals corrected LDA functionals with the density gradient.

- Meta-generalized gradient approximation (meta-GGA): functionals corrected GGA functionals with the kinetic energy density.
- Hybrid functional: functionals mixed the Hartree–Fock exchange integral at a constant ratio.
- Semiempirical functionals: functionals that reproduce accurate properties with many semi-empirical parameters.
- Progressive functionals: functionals transforming with combined functionals

2.2.3 Basis set

The basis sets are the most important input data for computational models in the chemistry, materials, biology, and other science domains that utilize computational quantum mechanics methods [45]. It is the set of one-electron wave functions that are combined to give the molecular wave functions. The minimal basis set integrated the orbitals that were populated by electrons [46]. The minimal basis sets and extended basis sets, such as Gaussian-type orbitals (GTOs), Slater-type orbitals (STOs), double-zeta, triple-zeta, quadruple-zeta, split-valence, polarized, and diffuse, are used for approximate theoretical calculations.

CHAPTER III

CALCULATION DETAILS

3.1 FI catalysts

3.1.1 Computational models

The X-ray structure of the FI catalyst was reported in an octahedral dichloride complex (**Figure 13**, left). Methylaluminoxane (MAO) is the most widely used as an activator for olefin polymerization [47, 48]. In this present study, we employed MAO to generate the vacant site before the ethylene insertion. Thus, the reactant π -complex (**Figure 13**, right) was used as a starting structure to gain insight into the polymerization mechanism. According to the experimental activities with different transition metal (M) substitutions [19], M-1 is referred to the parent FI catalyst containing phenoxy-imine (O, N) ligands ($R_1 = \text{H}$, $R_2 = t\text{-Bu}$, $R_3 = \text{H}$). The M-3 is referred to as the FI catalyst ($R_1 = \text{para-allyloxy group (} p\text{-OAll)}$, $R_2 = t\text{-Bu}$, $R_3 = \text{H}$), which exhibited the highest activity among the Ti-FI series reported by Nikitin et al. [25].

The M-1 was used to investigate the reaction mechanism of ethylene polymerization with different groups of IV_B transition metals ($M = \text{Ti, Zr, Hf}$). Then, we employed the Ti-1 catalyst to study the effects of ligand substitutions by changing parent phenoxy-imine (O, N) to (O, P), (O, O), and (O, S) ligands. For the most active Ti-3 (O, N), the most stable ligand from Ti-1 was applied to examine the effect of the ligand. Finally, the M-3 model was applied to the nickel (II) complexes based on the (O, N) ligand system.

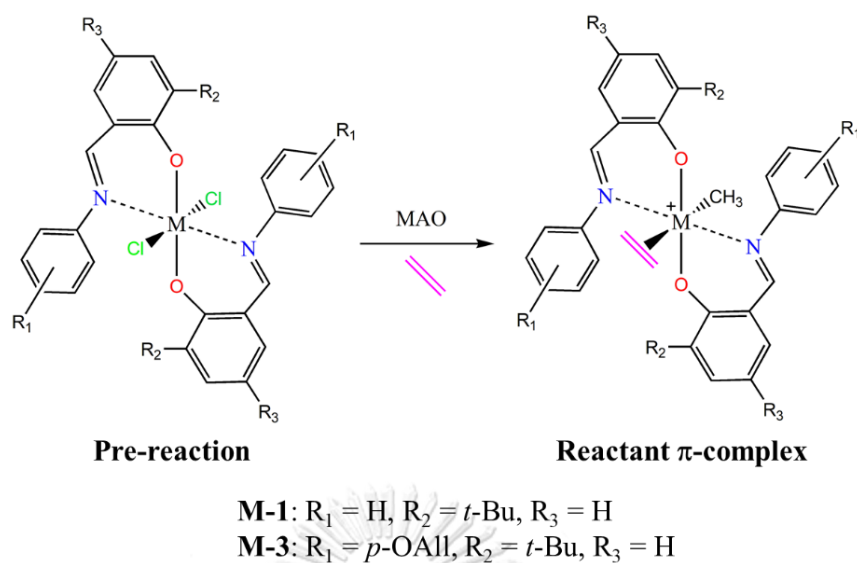


Figure 13 The FI catalyst's molecular structure for the pre-reaction complex (left) and the reactant π -complex (right). Where M is group IV_B transition metals (Ti, Zr, Hf).

Based on the proposed reaction mechanism as shown in **Figure 8**, the activation energy and reaction energy, represented as E_a and ΔE_r , are calculated according to **Equations (3.1)** and **(3.2)**.

$$E_a = E_{\text{TS}} - E_{\text{R}} \quad (3.1)$$

$$\Delta E_r = E_{\text{P}} - E_{\text{R}} \quad (3.2)$$

where E_{R} , E_{TS} , and E_{P} are the energies of the reactant π -complex (R), transition-state (TS), and the β -agostic product (P) for the ethylene insertion. The subscripts 1 and 2 refer to the first and second ethylene insertions, respectively.

3.1.2 DFT calculations

Several quantum calculations were performed to study the ethylene polymerization reaction [25, 49]. Hence, to validate the accuracy of our model, the octahedral dichloride complex of Ti-FI was optimized using the Gaussian 09 software [50], and the optimized structure was compared with the X-ray structure [18]. The cc-pVDZ basis set of Dunning [51] was used for non-metal atoms and the effective core potential (ECP)/LANL2DZ basis set [52] was used for transition metal atoms. Our

calculations were performed in gas phase conditions. The optimized stationary and transition state structures were confirmed by their vibrational frequency calculations with zero and one imaginary frequency. Moreover, the transition state structures were verified by intrinsic reaction coordinate (IRC) calculations. The self-consistent reaction field (SCRF) method was performed using the SMD solvation model [53].

Table 1 Comparison of bond distances (Å) and bond angles (°) of the pre-reaction complex (Ti-1) between X-ray structure [18] and seven theoretical methods with the cc-pVDZ basis set.

Bond distances (Å)	X-ray [18]	M06-						
		HF	B3LYP	BP86	M06	2X	M06L	MP2
Ti-O	1.85	1.84	1.87	1.88	1.86	1.85	1.87	1.85
Ti-N	2.24	2.23	2.28	2.27	2.26	2.26	2.28	2.27
Ti-Cl	2.31	2.29	2.27	2.28	2.26	2.25	2.27	2.27
Bond angles (°)	X-ray [18]	M06-						
		HF	B3LYP	BP86	M06	2X	M06L	MP2
O-Ti-O	171.6	168.6	169.6	170.6	168.2	168.6	168.5	166.1
N-Ti-N	76.4	85.4	77.7	76.8	75.9	74.0	73.9	71.3
Cl-Ti-Cl	103.1	99.6	103.5	104.3	104.5	104.8	104.8	106.3

Seven theoretical methods, i.e., HF, B3LYP, BP86, M06, M06-2X, M06L, and MP2 were employed. The comparison of bond lengths and bond angles with different theoretical methods is given in **Table 1**. We found that using M06-2X, similar to our previous work [54], shows good agreement with the X-ray structure. In addition, the hybrid-meta exchange correlation functionals M06-2X displayed good performance in describing thermochemistry, kinetics, and non-covalent interactions compared with other methods [55].

3.2 Ni-PEG catalysts

3.2.1 Computational models

Using X-ray structures of Ni-PEG with alkali metals (M) [6, 22], pre-reaction structures (**Figure 14**, left) with two different geometric isomers (A and B) were optimized. According to an experiment, phosphine abstraction is the first step in the activation process. From the ^{31}P NMR spectroscopy [22], the PMe_3 group can easily be removed from the nickel center. Thus, it is possible to generate a vacant site for ethylene insertion. Generally, the migratory insertion is responsible for the growth of the alkyl chain [56], while no evidence has been reported for the coordination with the phenyl group during polymerization [22]. In this study, we employed CH_3 and C_3H_7 for the R group as growing chains for the first and second ethylene insertions, respectively. Thus, the ethylene insertion complex model (**Figure 14**, right) was used as a starting structure to study the reaction mechanism of the Ni-PEG catalysts for ethylene polymerization.

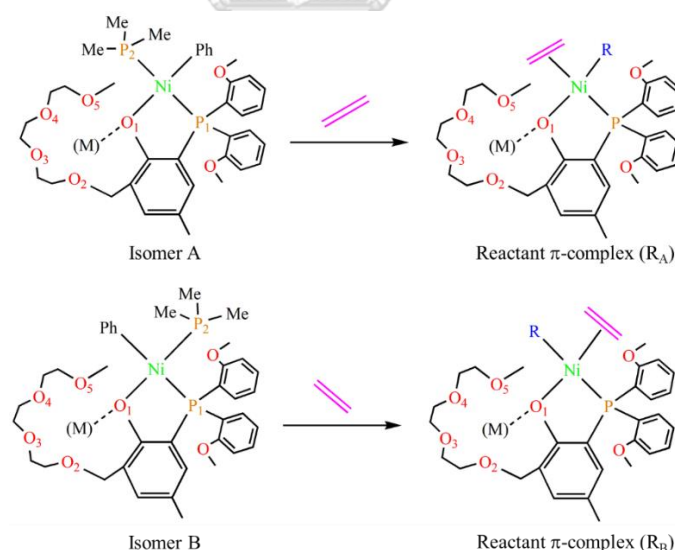


Figure 14 Heterobimetallic Ni-PEG with alkali metals (M = Li, Na, K, and Cs) for pre-reaction model (left) and for reaction pathway model (ethylene insertion complex, right). The geometric isomers A (top) and B (bottom) were defined. R = CH_3 and R = C_3H_7 as a growing chain for the first and second ethylene insertions, respectively.

Based on the proposed reaction mechanism in **Figure 9**, the activation energy ($E_{a1(A-B)}$), isomerization activation energy ($E_{a(iso1)}$), unfavorable route activation energy ($E_{a1(A)}$), favorable route activation energy ($E_{a1(B)}$), reaction energy (ΔE_{r1}), and β -hydrogen elimination step activation energy (E_{a12}) were calculated using **Equations (3.3) to (3.8)**:

$$E_{a1(A-B)} = E_{TS_B} - E_{R_A} \quad (3.3)$$

$$E_{a(iso1)} = E_{TS_{iso}} - E_{R_A} \quad (3.4)$$

$$E_{a1(A)} = E_{TS_A} - E_{R_A} \quad (3.5)$$

$$E_{a1(B)} = E_{TS_B} - E_{R_B} \quad (3.6)$$

$$\Delta E_{r1} = E_{P_B} - E_{R_A} \quad (3.7)$$

$$E_{a12} = E_{TS_{BA}} - E_{P_B} \quad (3.8)$$

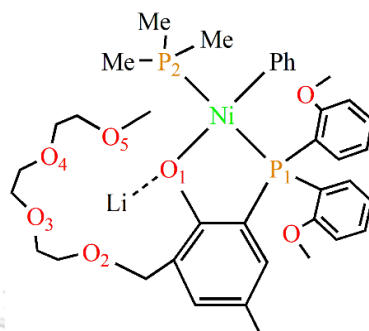
The $E_{a1(A-B)}$ for ethylene polymerization catalyzed by Ni-PEG with different alkali metals ($M = \text{Li, Na, K, and Cs}$) was first determined to compare with experimental activities [22]. The subscripts 1 and 2 refer to the first and second ethylene insertions, respectively.

3.2.2 DFT calculations

The calculations were performed using the Gaussian16 software [57]. DFT calculations were carried out with the wb97XD functional [58] and the 6-31G (d) basis set [59] for C, H, O, P, Li, Na, K, Be, Mg, Ca, Co, and Zn atoms, as well as the effective core potential (ECP)/SDD basis set [60] for Ni, Sr, and Cs atoms. The optimized Ni-PEG (Li) with different method/basis sets were compared with the X-ray structures [22] and are shown in **Table 2**. All the optimized stationary and transition state structures were confirmed by zero and one imaginary frequency, respectively, in normal mode analysis. The process from reactant π -complex–TS– β -agostic product was verified by intrinsic reaction coordinate (IRC) calculations. The structures were calculated in gas phase conditions. For the pre-reaction state, some selected key bond parameters in the optimized structures were examined to find the correlation between the catalyst

structure and experimental activities. Moreover, natural population analysis (NPA) [61] was performed for the natural atomic charges (NBO).

Table 2 Bond lengths (Å), bond angles (°), dihedral angles (°) of isomer A's optimized Ni-PEG(Li) structure with different method/basis set.



Represent structure of isomer A of Ni-PEG(Li)

Parameters	X-ray [22]	B3LYP-D3/ 6-31G(d) & Lanl2DZ [22]		ωB97XD/ 6-31G(d) & Lanl2DZ		ωB97XD/ 6-31G(d) & SDD (In this work)		ωB97XD/ 6-31G (d,p) & SDD	
		B3LYP/ 6-31G(d) & Lanl2DZ	ωB97XD/ 6-31G(d) & Lanl2DZ	ωB97XD/ 6-31G(d) & Lanl2DZ	ωB97XD/ 6-31G(d) & SDD (In this work)	ωB97XD/ 6-31G (d,p) & SDD			
Ni - P ₁	2.19	2.26	2.29	2.24	2.22	2.22			
Ni - O ₁	1.94	2.04	1.99	1.95	1.94	1.94			
Ni - C _{ph}	1.89	1.90	1.91	1.89	1.89	1.89			
Ni - P ₂	2.19	2.24	2.27	2.22	2.21	2.21			
Li - O ₁	1.93	1.91	1.93	1.90	1.91	1.91			
Ni - Li	3.21	3.32	3.37	3.13	3.14	3.13			
Ni-O ₁ -Li	112.0	114.4	118.5	108.7	109.3	109.0			
P ₁ -Ni-P ₂	168.5	170.9	168.7	171.2	171.1	171.1			
Li-O ₁ -Ni-C _{ph}	5.4	-8.1	-12.9	28.9	28.0	31.5			
P ₂ -Ni-O ₁ -Li	79.7	76.7	75.9	76.7	75.6	75.3			

CHAPTER IV

RESULTS AND DISCUSSION

4.1 FI catalysts

4.1.1 Stability of pre-reaction complexes

Phenoxy-imine with group IV_B transition metal complexes having an octahedral geometry. Around the metal (M) center, the structures are connected with two imine nitrogens, two phenolic oxygens, and two chloro ligands. There were five possible isomers of pre-reaction Ti-FI complexes with different rearrangements: *cis-N/trans-O/cis-Cl* (isomer A), *cis-N/cis-O/cis-Cl* (isomer B), *trans-N/cis-O/cis-Cl* (isomer C), *cis-N/cis-O/trans-Cl* (isomer D), and *trans-N/trans-O/trans-Cl* (isomer E) [2] were employed to evaluate the stability of pre-reaction complexes. The relative potential energy (RE) of the five possible isomers is given in **Figure 15**. Our calculation results revealed that isomer A is the most stable form (RE = 0.0 kcal mol⁻¹), followed by isomer B (RE = 2.0 kcal mol⁻¹), D (RE = 6.6 kcal mol⁻¹), C (RE = 7.9 kcal mol⁻¹), and E (RE = 11.2 kcal mol⁻¹), respectively. The relative stabilities show similar results with the Zr-FI complexes by indicating that the structure *cis-N/trans-O/cis-Cl* (isomer A) was found to be the most preferred [62]. Moreover, isomer A corresponds to an X-ray structure [18]. From our observation, the octahedral geometry in isomer A's structure allows the polymer chain and ethylene monomer to be inserted into the *cis*-position easier than other isomers. Hence, the isomer A is used to investigate the reaction mechanism in the next section.

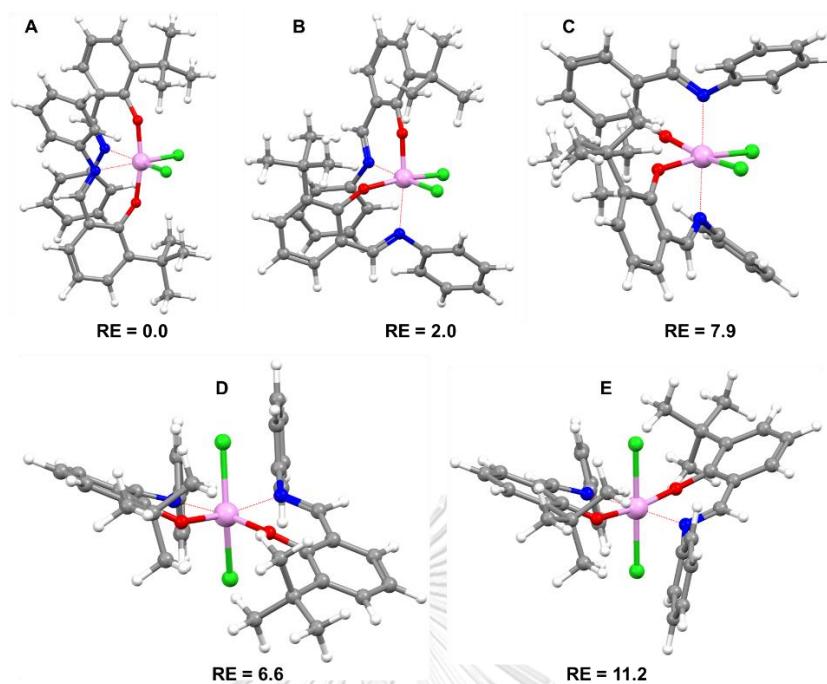


Figure 15 The relative potential energy (RE) in kcal mol⁻¹ of the five possible isomers (A-E) at the pre-reaction Ti-FI states. Isomer A is the most stable and is the reference.

4.1.2 Effect of metal substitutions

Before studying the reaction mechanism, the most stable octahedral dichloride complex isomer A was activated by MAO. Then, the cationic FI catalyst was created to represent the catalyst with one vacant site as the starting point for the polymerization reaction with the ethylene monomer. The methyl and propyl groups were used to model the growing polymer chains for the first and second ethylene insertions.

Since the ethylene polymerization activity of general FI catalysts (M-1) with different metal substitutions was reported by Mitani et al. [19] The highest activity was obtained by using Zr-1 as the metal center, followed by Hf-1 and Ti-1, respectively. In this part, we investigated the reaction mechanism and examined the effect of group IV_B transition metals (M = Ti, Zr, Hf) substitutions on phenoxy-imine (FI) catalysts for ET polymerization based on our proposed mechanism as depicted in **Figure 8** using the DFT calculations.

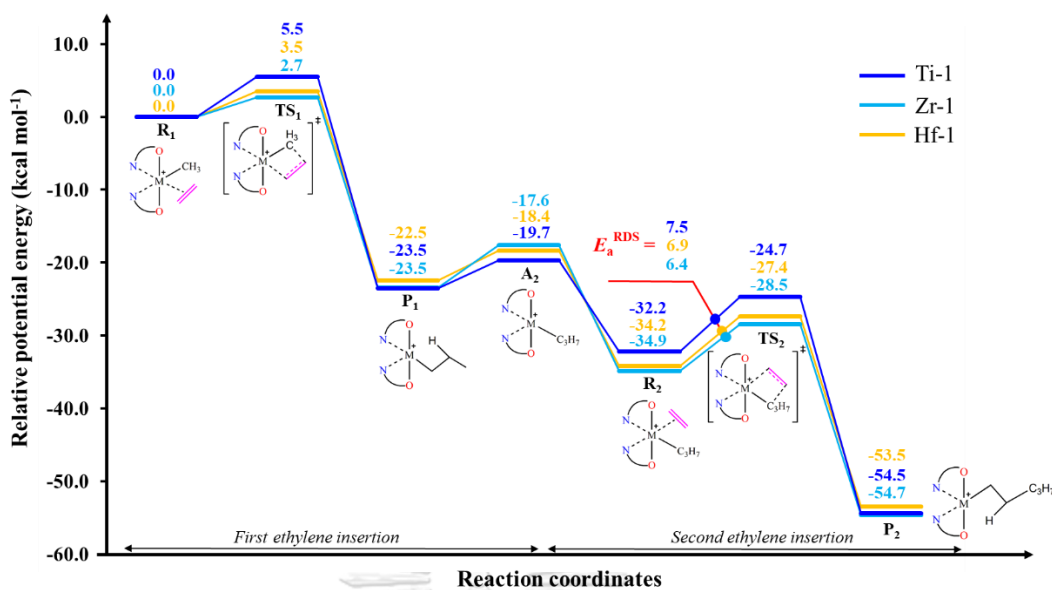


Figure 16 Relative potential energy profiles of ethylene polymerization by the FI catalysts. Different groups of IV_B (Ti, Zr, Hf) transition metals were compared. The potential energies relative to R₁ are given in kcal mol⁻¹.

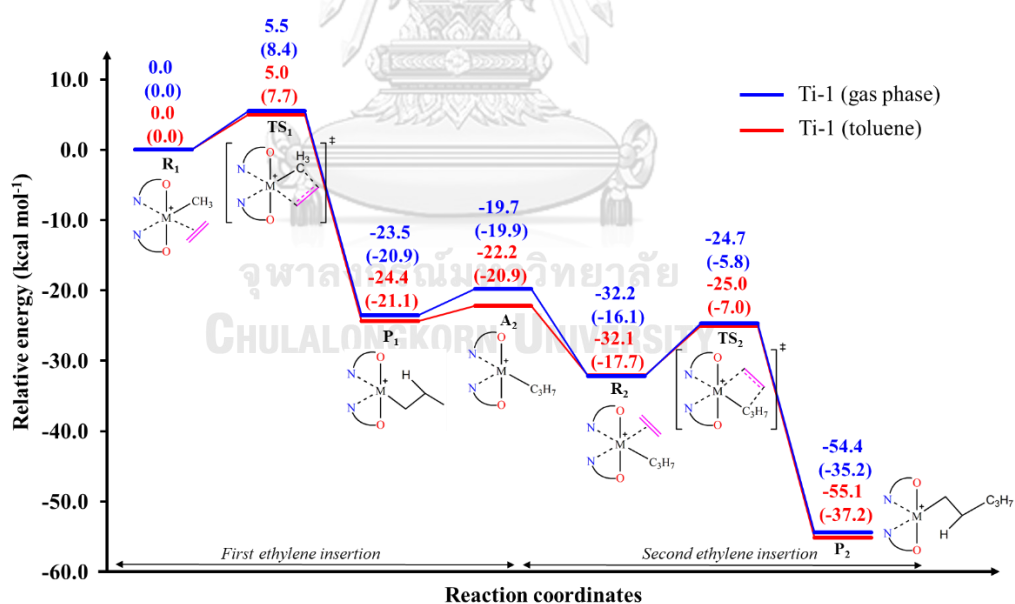


Figure 17 Relative energy profiles for ethylene polymerization catalyzed by (Ti-1)-FI catalyst in the gas phase (blue line) and toluene (red line). The energies relative to R₁ are given in kcal mol⁻¹. The relative Gibbs free energy (ΔG[‡]) at 298.15 K is shown in parenthesis.

The relative potential energy profiles of ET polymerization by the FI catalysts are shown in **Figure 16**. From the starting complex R_1 to P_1 of the first ethylene insertion, the activation energies (E_{a1}) are 5.5, 2.7, and 3.5 kcal mol⁻¹ and the reaction energies (ΔE_{r1}) are -23.5, -23.5, and -22.5 kcal mol⁻¹ for Ti-1, Zr-1, and Hf-1, respectively. For the second ethylene insertion, the activation energies (E_{a2}) are 7.5, 6.4, and 6.9 kcal mol⁻¹ and the reaction energies (ΔE_{r2}) are -22.2, -19.8, and -19.3 kcal mol⁻¹ for Ti-1, Zr-1, and Hf-1, respectively. In addition, the Gibbs free energy profiles at 298.15 K and 1 atm were reported in both gas phase and toluene solvent as given in **Figure 17**. The experimental activities and our DFT calculation results are shown in **Table 3**.

Table 3 Experimental activities and our DFT calculation results. The energies are given in kcal mol⁻¹.

Metals	Experimental results		DFT calculation results				
	Activity (kg mmol ⁻¹ h ⁻¹)	log activity	E_{a1}	E_{a2}	$E_{(A2-P1)}$	ΔE_{r1}	ΔE_{r2}
Ti	3.3	0.52	5.5	7.5	3.8	-23.5	-22.2
Zr	519.0	2.72	2.7	6.4	5.9	-23.5	-19.8
Hf	6.5	0.81	3.5	6.9	4.1	-22.5	-19.3

Conditions: co-cat. MAO, 25°C, $p(C_2H_4)$ 0.1 MPa. E_{a2} is the RDS.

It was found that the trends of E_{a1} and E_{a2} , which Zr-1 < Hf-1 < Ti-1, showed good agreement with experimental activities. The highest energy is displayed for the second ethylene insertion. Thus, the second insertion is the rate-determining (RD) step of this reaction, which corresponds to [25]. Therefore, the structures related to the second ethylene insertion were further investigated as the key factors of ET polymerization by the FI catalyst. In addition, the reaction energy exhibited an exothermic process for both the first and second insertions. However, the trend of ΔE_{r1} and ΔE_{r2} is not related to experimental activities.

According to the RD step, the R_2 - TS_2 - P_2 structures were mainly focused on determining the factors that related to the experimental activities as well as the E_a^{RDS}

and E_r^{RDS} . From the structures, the distance between the transition metal center (M) and nitrogen (at the nearest ethylene insertion site) is possibly related to the catalytic activities. The M-N distance for the TS_2 structures was found to be Zr-N (2.34 Å) > Hf-N (2.30 Å) > Ti-N (2.23 Å) and Zr-N (2.28 Å) > Hf-N (2.24 Å) > Ti-N (2.10 Å), which showed a similar trend to experimental activity. In contrast to the M-N distance trend of R_2 structures, Zr-N (2.36 Å) = Hf-N (2.36 Å) > Ti-N (2.24 Å).

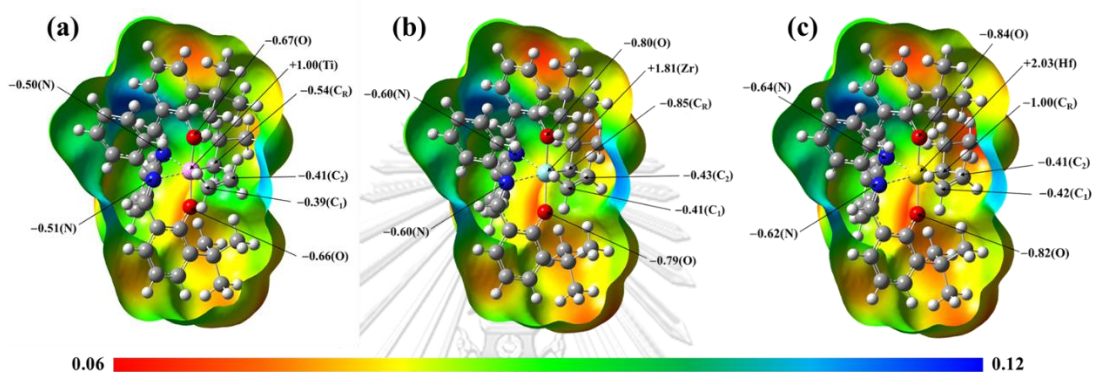


Figure 18 The molecular electrostatic potential (MEP) maps and NBO charges of (a) (Ti-1)-FI (b) (Zr-1)-FI (c) (Hf-1)-FI of the reactant π -complex (R_2). The isosurface value is 0.002, with a range for the MEPs map of 0.06 to 0.12 a.u.

Then, we employed the molecular electrostatic potential (MEP) maps and NBO charges of the R_2 structures to clarify the factors that affected catalytic activity, as shown in **Figure 18**. The NBO charges are in the order of Hf-FI (+2.03) > Zr-FI (+1.81) > Ti-FI (+1.00). We found that the electrostatic and electronic effects are not related to the trend of experimental activities, but they do correspond to the size of metal cations. Therefore, the structural M-N distance parameter would be focused on determining the key factors for ET polymerization. We summarized that the elongation of the M-N distances provided a larger space and, consequently, the ethylene monomer could easily insert the metal center.

4.1.3 Effect of ligand substitutions

In the previous part, the parent (Ti-1)-FI catalyst containing (O,N) ligands exhibited the highest activation energy at the RD step among group IV_B transition metals. Therefore, by changing heteroatom (O, X) on ligands from nitrogen (O, N) into oxygen (O, O), phosphorus (O, P) and sulfur (O, S), the catalytic activities are possibly improved.

Table 4 The calculated activation energy (E_a^{RDS}) and reaction energy (ΔE_r^{RDS}) of different ligand substitutions of Ti-1 (O, X) and Ti-3 (O, X) systems at the rate-determining step.

Energy (kcal mol ⁻¹)	Ti-1 (O, X) system				Ti-3 (O, X) system	
	(O, N)	(O, P)	(O, O)	(O, S)	(O, N)	(O, S)
E_{a2}^{RDS}	7.5	4.7	5.0	2.2	4.2	2.4
ΔE_{r2}^{RDS}	-28.1	-24.3	-22.1	-19.6	-23.6	-19.3

Table 4 displays the calculated activation energy (E_a^{RDS}) and reaction energy (ΔE_r^{RDS}) of the different ligand substitutions at the RD step. For the Ti-1 catalyst using (O, N), (O, P), (O, O), and (O, S) ligands with the E_a^{RDS} values of 7.5, 4.7, 5.0, and 2.3 kcal mol⁻¹ and the ΔE_r^{RDS} values of -28.1, -24.3, -22.1, and -21.7 kcal mol⁻¹, respectively. The results revealed that by substitution with P, O, and S for the Ti-1 system can decrease the E_a^{RDS} as well as obtain a less exothermic reaction. By using P, O, and S instead of N, they can provide a more potent catalyst than the parent Ti-1 system. The lowest activation energy was found in the Ti-1 (O, S) system, which indicated the highest potency for improving catalytic activities. For the Ti-3 catalyst using (O, N) and (O, S) ligands with the E_a^{RDS} values of 4.2 and 2.4 kcal mol⁻¹ and the ΔE_r^{RDS} values of -23.6 and -19.3 kcal mol⁻¹, respectively. The E_a^{RDS} of Ti-3 (O, N) is lower than that of Ti-1, which is in accordance with experimental activities reported by Nikitin et al. [25]. Moreover, the Ti-1 (O, S) still provided lower E_a^{RDS} than the Ti-1 (O, N) and Ti-3 (O, S). The results correspond to those of Lapenta et al. [63], which suggest that using (O, S) ligands contributes to a highly active catalytic system.

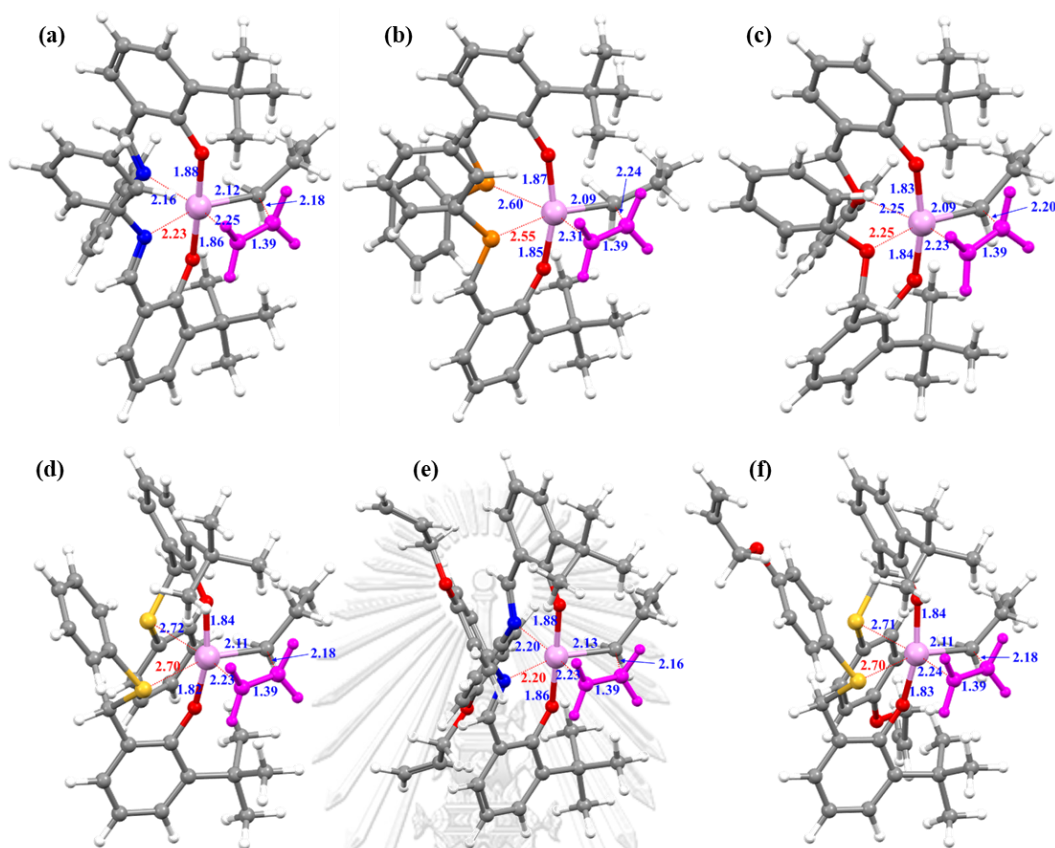


Figure 19 Optimized TS structures of Ti-1 with (a) (O, N) (b) (O, P) (c) (O, O) (d) (O, S) ligands and Ti-3 with (e) (O, N) (f) (O, S) ligands. The carbon, hydrogen, oxygen, nitrogen, phosphorus, sulfur, and titanium atoms are shown in grey, white, red, blue, orange, yellow, and light pink, respectively. The ethylene (ET) molecule is shown in a dark pink. Distances (Å) are given in blue and red.

According to the previous part, we suppose that the M-N distance plays a key role in controlling the catalytic activity. Hence, the distance between titanium and the heteroatom (Ti-X) was mainly determined. **Figure 19a-d** displays the optimized TS structures of Ti-1 with (O, N), (O, P), (O, O), and (O, S) ligands. The Ti-X distance is proportional to the activation energy in the following order: Ti-S (2.70 Å) > Ti-P (2.55 Å) > Ti-O (2.25 Å) > Ti-N (2.23 Å). The longest Ti-S distance indicated that the weak interaction between the metal center and the heteroatom easily generated the Ti-ET formation and forwarded the polymerization reaction as a result of the lowest E_a^{RDS} .

Moreover, the optimized TS structures of Ti-3 with (O, N) and (O, S) ligands were employed as shown in **Figures 19e and 19f**. The calculation results show that the Ti-X distance of the Ti-3 catalyst using the (O, N) and (O, S) ligands is 2.20 Å and 2.70 Å, respectively. As a result, we can conclude that the M-X distance is critical in the design of Ti (O, X)-FI-based catalysts. Furthermore, our calculations revealed that all of the product structures had a strong β -agostic interaction, as evidenced by the elongated C_R-H_β bond distance (1.13-1.15 Å) compared to the standard C-H bond distance of 1.10 Å [64].

4.1.4 Novel Ni-phenoxy-imine (Ni-FI) catalysts with (O, N) ligand

Nikitin et al. [25] have collected the experimental activity data of the phenoxy-imine titanium catalysts for ethylene polymerization. From their report, the Ti-phenoxy-imine (Ti-3) catalyst with (O, N) ligand is the most active FI catalyst. Recently, Chasing et al. [28] have proposed nickel (II) complexes based on the phenoxy-imine (O, N) ligand as candidate catalysts for ethylene polymerization. Thus, in this work, we have calculated the activation energy at the RD step of the Ni-phenoxy-imine (Ni-FI) catalyst by using Ti-3 as the template catalyst. Our calculation results revealed that the E_a^{RDS} of the Ni-FI catalyst has very high activation energy ($E_a^{RDS} = 29.6 \text{ kcal mol}^{-1}$) and the ΔE_r^{RDS} of $-22.4 \text{ kcal mol}^{-1}$. From our observation, the high E_a^{RDS} value comes from the C_2 symmetric octahedral geometry of the Ni-FI catalyst, which is in accordance with the literature review reported [2]. This type of Ni-FI catalyst is an inactive catalyst for the ethylene polymerization [65]. The result when we calculated the nickel (II) complexes based on the phenoxy-imine (O,N) ligand in a square planar half-geometry was quite interesting. Then, we found that the E_a^{RDS} of half the Ni-FI catalyst was decreased to $12.3 \text{ kcal mol}^{-1}$ and the ΔE_r^{RDS} is exothermic with $-20.8 \text{ kcal mol}^{-1}$.

On the other hand, the E_a^{RDS} and ΔE_r^{RDS} of the half (Ti-3)-FI complex are 11.7 and $-8.8 \text{ kcal mol}^{-1}$, which are calculated from the optimized geometry R_2 , TS_2 , and P_2

of the ET polymerization catalyzed by the half (Ti-3)-FI complex shown in **Figure 20**. It is clearly seen that the Ni-FI in a square planar geometry provided a stronger interaction between ET and the Ni metal center. Therefore, the DFT results suggest the geometry of the nickel (II) complexes based on the phenoxy-imine (O, N) ligand in half-geometry is more reactive than the C_2 symmetric octahedral geometry.

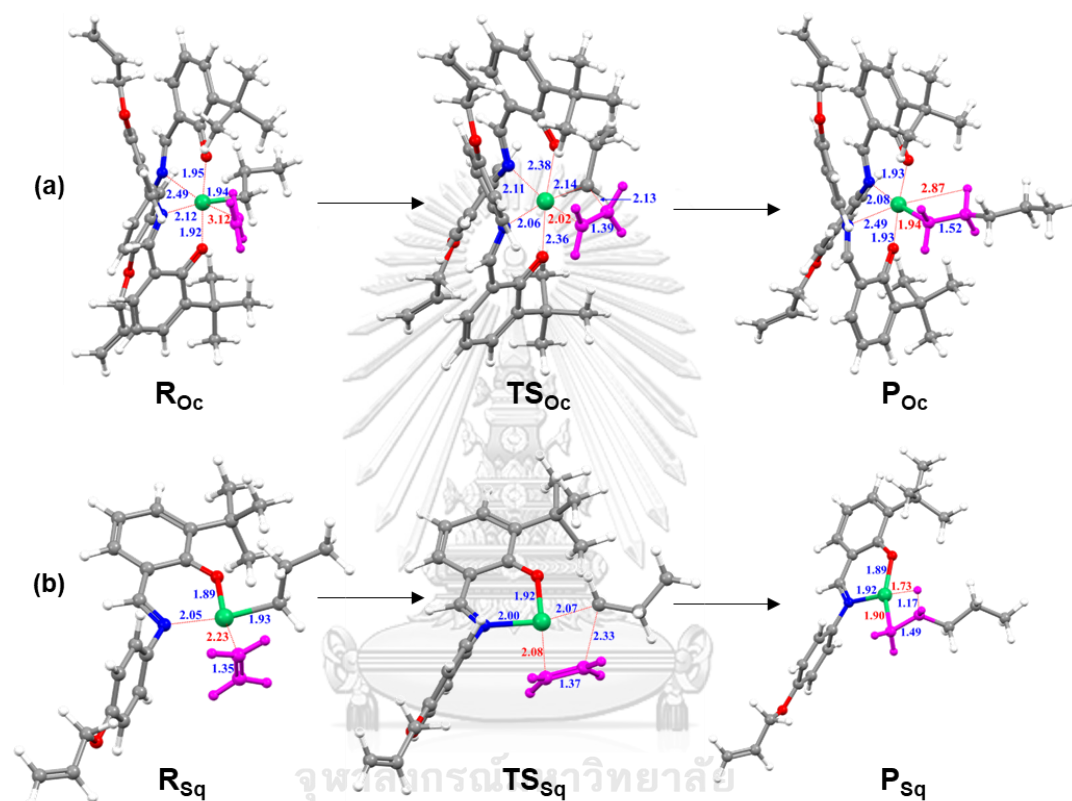


Figure 20 Optimized structures of the reactant π -complex (R), transition state (TS), and β -agostic product (P) for the ethylene polymerization catalyzed by (a) octahedral Ni-FI and (b) square planar of half Ni-FI. Bond distances (Å) are displayed in blue and red.

4.2 Ni-PEG catalysts

The ethylene polymerization catalyzed by nickel (II) complexes based on the phenoxy-imine (O, N) ligand in half-geometry has been investigated in several papers [66-68]. However, some of their common limitations are that they exhibit moderate activity, produce short chain polymers, and have poor control over polymer

microstructures [6]. In addition, FI catalysts were specifically group IV_B transition metal, phenoxy-imine ligands, and their geometry, which are limited for catalyst design. Hence, heterobimetallic Ni-PEG [22, 27], which provides the highest ethylene polymerization activity among Ni-based FI catalysts, has been focused on. The DFT calculations were performed to examine our proposed mechanism for ethylene polymerization catalyzed by Ni-PEG. Firstly, relative potential energy profiles for ethylene polymerization by each Ni-PEG catalyst in favorable pathways were focused. Then, the effects of catalyst structures on experimental activities were elucidated.

4.2.1 Reaction pathways of Ni-PEG(M) for ethylene polymerization

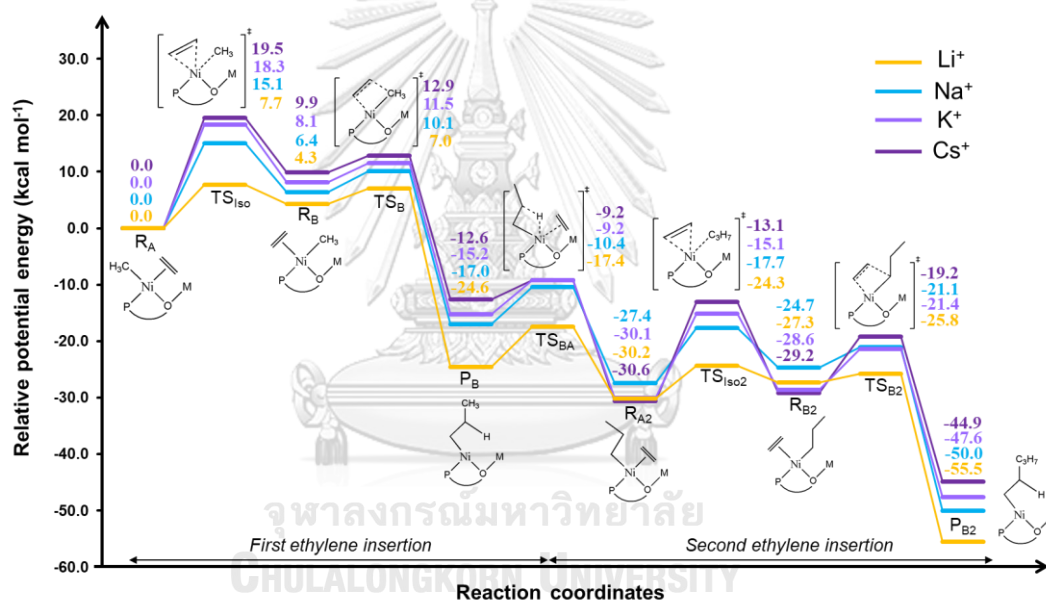


Figure 21 Relative potential energy profiles for ethylene polymerization catalyzed by Ni-PEG. Favorable pathways for alkali metals ($M = \text{Li}, \text{Na}, \text{K}, \text{and Cs}$) were compared. The potential energies relative to the complex R_A are given in kcal mol^{-1} .

From the starting complex R_A of the first ethylene insertion, the isomerization of the Ni complex generates R_B . The activation energy for the isomerization from R_A to R_B ($E_{a(\text{Iso1})}$) is 7.7, 15.1, 18.3, and 19.5 kcal mol^{-1} for $M = \text{Li}, \text{Na}, \text{K}, \text{and Cs}$, respectively. Then, the reaction proceeds along with R_B to P_B via TS_B with a small activation energy ($E_{a1(\text{B})}$). This is because the ethylene insertion into the *trans* position to the oxygen has

less steric hindrance. Because the reaction starting complex R_A is the more stable reactant, the energy difference between TS_B and R_A is defined as the activation energy ($E_{a1(A-B)}$). The $E_{a1(A-B)}$ values for Ni-PEG with Li, Na, K, and Cs are 7.0, 10.1, 11.5, and 12.9 kcal mol⁻¹, respectively. The reaction energy (ΔE_{r1}), an energy difference between P_B and R_A , was calculated to be -24.6, -17.0, -15.2 and -12.6 kcal mol⁻¹ for M = Li, Na, K, and Cs, respectively. The ΔE_{r1} showed that the first ethylene insertion step is an exothermic process, which is similar to that obtained from the previous DFT study for the reaction mechanism of the palladium-catalyzed ethylene polymerization by Masaev et al [69]. The R_A to P_B reaction with Ni-PEG(Li) is the most exothermic when compared with the other three alkali metal systems. This is because the distance between secondary metal (M) and oxygen of the PEG group ($M-O_{PEG}$) in the Li system significantly decreases when the reaction proceeds from R_A to P_B . The activation energies from P_B to R_{A2} via $TS_{BA}(E_{a12})$, β -hydrogen elimination step, for complexes with M = Li, Na, K, and Cs were found to be 7.2, 6.5, 5.9, and 3.4 kcal mol⁻¹, respectively. Thus, with Ni-PEG (Cs), the reaction is the easiest to forward to R_{A2} because it has the smallest activation energy. The process is continued from R_{A2} to P_{B2} in a similar manner to the first ethylene insertion.

For the second ethylene insertion, in the respective orders for Ni-PEG with Li, Na, K, and Cs, the $E_{a(iso2)}$, is 5.9, 9.7, 15.0, and 17.5 kcal mol⁻¹, the $E_{a2(A-B)}$, is 4.4, 6.3, 8.6, and 11.4 kcal mol⁻¹, and the ΔE_{r2} , is -25.2, -22.6, -17.5, and -14.3 kcal mol⁻¹. Trends for $E_{a(iso2)}$ and $E_{a2(A-B)}$ in the second ethylene insertion are similar to those for $E_{a(iso1)}$ and $E_{a1(A-B)}$ in the first insertion.

Based on the relative potential energy profiles in **Figure 21**, the $E_{a(iso1)}$ provided the highest energy barrier for ethylene polymerization catalyzed by Ni-PEG for all the systems. Thus, the isomerization step is the rate-determining step of this reaction. This is consistent with the experimental results, i.e., the preference of isomer A for Ni-PEG (Li) and Ni-PEG (Cs) and the preference of isomer B for Ni-PEG (Na) and Ni-PEG (K). However, our calculation models for the reaction pathway are different from the pre-

reaction model. Our calculations indicated that the ethylene insertion into the *cis* position relative to the oxygen is favored over its isomer. Hence, the R_A is more stable than the R_B for all systems. However, the polymerization reaction preferred ethylene insertion into the *trans* position to the oxygen due to the less steric hindrance, which makes the $E_{a1(B)}$ possess a small activation energy. Therefore, the isomerization step is always required for Ni-PEG before the polymerization reaction takes place. Previous studies [69] have reported that the first ethylene insertion is the rate-determining step for the ethylene polymerization reaction. However, they did not include the isomerization step. To study the preference of isomers on cations, the $E_{a1(A-B)}$, which refers to the activation energy from R_A to polymerization reaction via TS_B , including the isomerization step, was used to compare with experimental activities [22]. The optimized structures of R_A and TS_B for ethylene polymerization by Ni-PEG catalysts with different alkali metals (M) are shown in **Figure 22**.

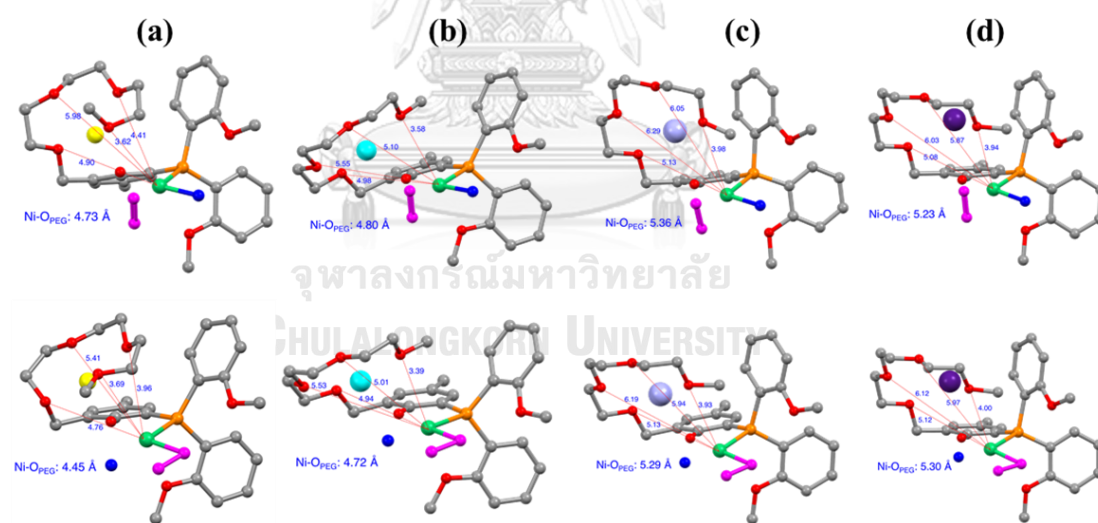


Figure 22 Optimized structure of the reactant (R_A) and transition state (TS_B) for ethylene polymerization by Ni-PEG catalysts with different alkali metals (M) (a) Li (b) Na (c) K, and (d) Cs for the first ethylene insertion ($R = CH_3$) of the favorable pathway. The H atoms were omitted for clarity.

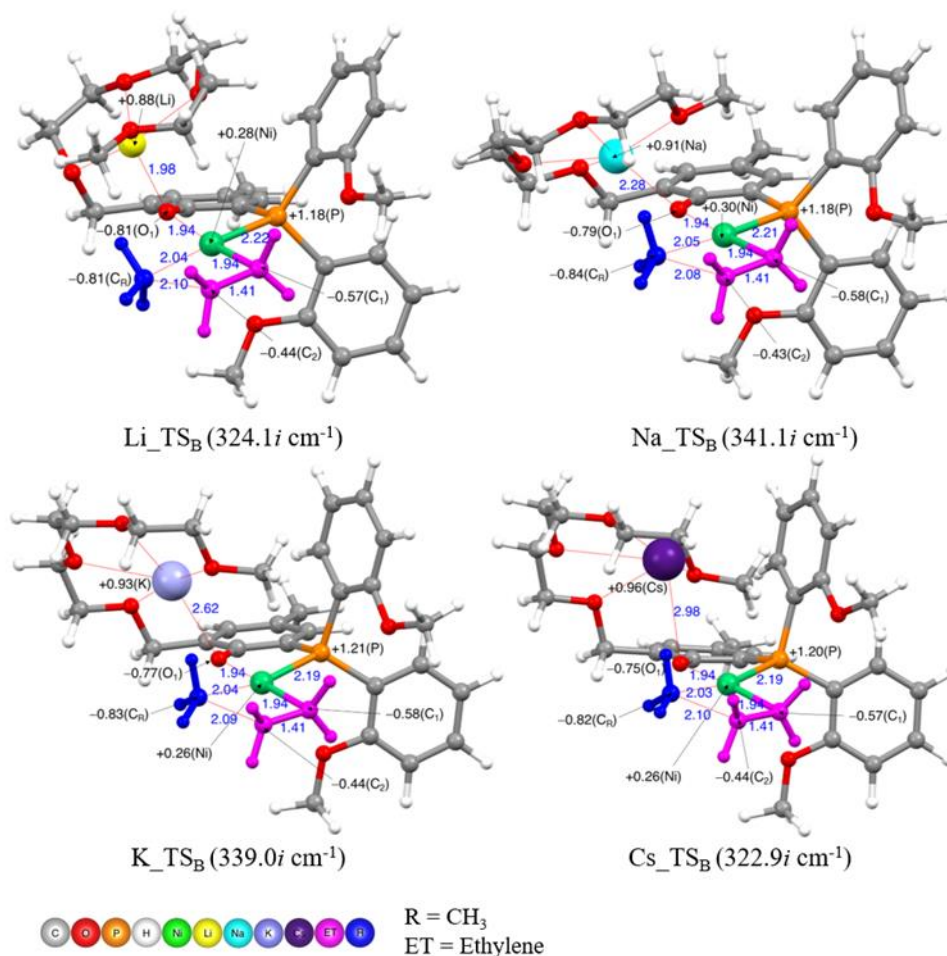


Figure 23 Optimized structure of transition state (TS_B) for ethylene polymerization by Ni-PEG catalysts with different alkali metals for the first ethylene insertion (R = CH₃) of the favorable pathway. Distances (Å) are given in blue, and NBO charges are shown in black.

The Ni-metal center plays an important role in ethylene (ET) polymerization. Thus, the interaction around Ni with the polymerization region was first determined. Optimized structures of the four-membered ring transition state (TS_B) for ethylene polymerization by the Ni-PEG catalysts with different alkali metals (M) for the first ethylene insertion (R = CH₃) of the favorable pathway are given in **Figure 23**. Bond distances and NBO charges were analyzed for both steric and electronic effects in four Ni-PEG systems. From analysis, the order is as follows: Ni-Li(3.48 Å) < Ni-Na(3.51 Å) < Ni-K(3.77 Å) < Ni-Cs(3.89 Å) for Ni-M distance and Li-O₁(1.98 Å) < Na-O₁(2.28 Å) < K-

$O_1(2.62 \text{ \AA}) < Cs-O_1(2.98 \text{ \AA})$ for $M-O_1$ distance. Moreover, the trend of NBO charges on M atoms is $Li(+0.88) < Na(+0.91) < K(+0.93) < Cs(+0.96)$. Interestingly, when Li is used as a secondary metal, the charge of O_1 atom is more negative (-0.81) than the charge of O_1 atom on $Na(-0.79)$, $K(-0.77)$, and $Cs(-0.75)$. As evidenced by strong interactions between metals, the Ni-M interaction suggests the significance of the cooperative effect in catalysts. The positive NBO charge on the cation tends to be affected by the metal-ligand interaction. The interaction between the metal and the PEG group might affect the charge on M and possibly relate to the rate of polymerization.

4.2.2 Influence of catalyst structures on experimental activity

In the last section, we focused on the pre-reaction state of the Ni-PEG catalysts. If there is a correlation between the structure of the pre-reaction state and experimental activity, the computational effort for a predictive study would be much less. Initially, our results revealed that Ni-PEG with Li and Cs are more stable in isomer A, whereas those with Na and K is more stable in isomer B. This suggestion corresponds to the experimental finding on the existing isomer A:B ratio. Then, we employed the most stable isomer to find the relationship between the catalyst structures and the experimental activities [22]. Selected bond lengths, bond angles, dihedral angles, and NBO charges of the optimized Ni-PEG catalysts were presented in **Table 5**.

Table 5 Selected bond lengths (Å), bond angles (°), dihedral angles (°), and NBO charges of Ni-PEG. When M = Li, Na, K, and Cs

M (Isomer)*	Li (A)	Na (B)	K (B)	Cs (A)
Activity**	35000	18000	2900	360
log(activity)	4.54	4.26	3.46	2.56
Ni - P ₁	2.22	2.26	2.27	2.21
Ni - O ₁	1.94	1.91	1.92	1.92
Ni - O _{PEG} ***	4.25	4.80	5.40	5.15
M - O ₁	1.91	2.22	2.62	3.12
M - O _{PEG} ***	2.11	2.41	2.77	3.15
Ni - M	3.14	3.28	3.68	3.67
Ni-O ₁ -M	109.3	104.4	107.4	90.1
P ₁ -Ni-P ₂	171.1	102.7	103.0	175.6
M-O ₁ -Ni-C _{Ph}	28.0	-50.0	43.3	30.4
q _{Ni}	+0.28	+0.24	+0.23	+0.21
q _{O1}	-0.87	-0.80	-0.79	-0.79
q _{OPEG} ***	-0.64	-0.63	-0.62	-0.61
q _M	+0.86	+0.91	+0.93	+0.99
q _{P1}	+1.11	+1.10	+1.09	+1.12

* Isomer = the most stable form of isomer

** Activity in kg mol⁻¹ h⁻¹ unit at the experimental temperature 30 °C

*** O_{PEG} = average of O₂-O₅ atoms

From the analysis, we found the best two parameters, the distance between the secondary metal (M) and O₁ of the phenoxyphosphine ligand (M-O₁) and the average distance between M and four oxygens (O₂-O₅ atoms) of the PEG group (M-O_{PEG}), with a high correlation to experimental activities [22]. The relationship between log(activity) and the M-O₁ and M-O_{PEG} distances was plotted in **Figure 24**. To ensure a high level of correlation with experimental activity, an R-square (R²) criterion of 0.8 was

used [70]. From **Figure 24**, plots of the $M-O_1$ and $M-O_{PEG}$ distance parameters with \log (activity) showed an R^2 of 0.98 and 0.97, respectively. Hence, these two key parameters could be used for the design and screening of potent Ni-PEG catalysts. To summarize, the potent Ni-PEG catalysts should have shorter $M-O_1$ and $M-O_{PEG}$ distances.

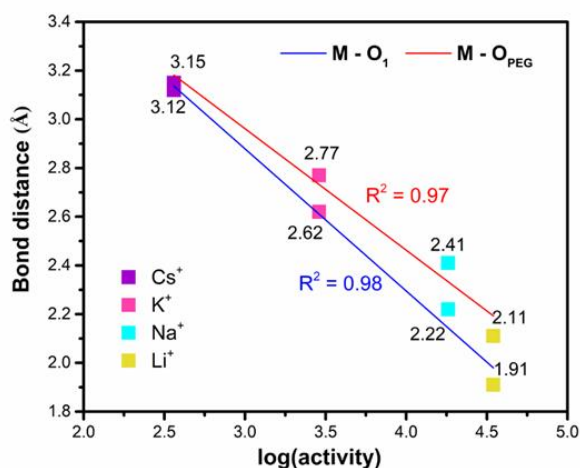


Figure 24 The relationship between \log (activity) and the $M-O_1$ and $M-O_{PEG}$ distances from the most stable isomer of Ni-PEG with four alkali metals (M cation).

Our study has also indicated that the catalyst with the shorter $M-O_{PEG}$ and $M-O_1$ distances has the most enhanced catalytic activity and that with Li has the shortest distances. Thus, it is interesting to use these geometrical parameters to predict the activity of Ni-PEG with other secondary metals, such as the divalent cation. Thus, the Ni-PEG with alkali-earth metals (Be, Mg, Ca, Sr) and other divalent transition metals such as Co and Zn were investigated in the same way as the Ni-PEG system.

The optimized structures of Ni-PEG catalysts with M^{2+} cations (Be, Mg, Ca, Sr, Co, and Zn) were compared with the Ni-PEG (Li) complex and demonstrated in **Figure 25a-g**. The $M-O_1$ distances for Ni-PEG with Be, Mg, Ca, Sr, Co, and Zn are 1.59, 1.94, 2.32, 2.42, 1.91, and 1.89 Å, respectively. The $M-O_{PEG}$ distances for Ni-PEG with Be, Mg, Ca, Sr, Co, and Zn are 1.85, 2.13, 2.47, 2.60, 2.17, and 2.13 Å, respectively. Calculated values for $M-O_1$ and $M-O_{PEG}$ of Ni-PEG with Mg, Co, and Zn are close to those of Ni-PEG (Li). This suggests that the catalyst with Mg, Co, and Zn as the secondary metals could

also yield high activity. On the other hand, the Ni-PEG (Be) exhibited the shortest distance for both $M-O_1$ and $M-O_{PEG}$. Thus, the PEG group in this catalyst is in the most compact form and shows the strongest metal-ligand interaction. Therefore, the Ni-PEG catalyst with Be cation is the most promising candidate. Recently, Xiao et al. [71] have reported that nickel complexes with phosphine phosphonate-PEG ligand in combination with Co and Zn cations can enhance the rate of polymerization. This finding agrees with our results. Our study, therefore, provided key concepts for designing highly active catalysts for ethylene polymerization based on Ni-PEG.

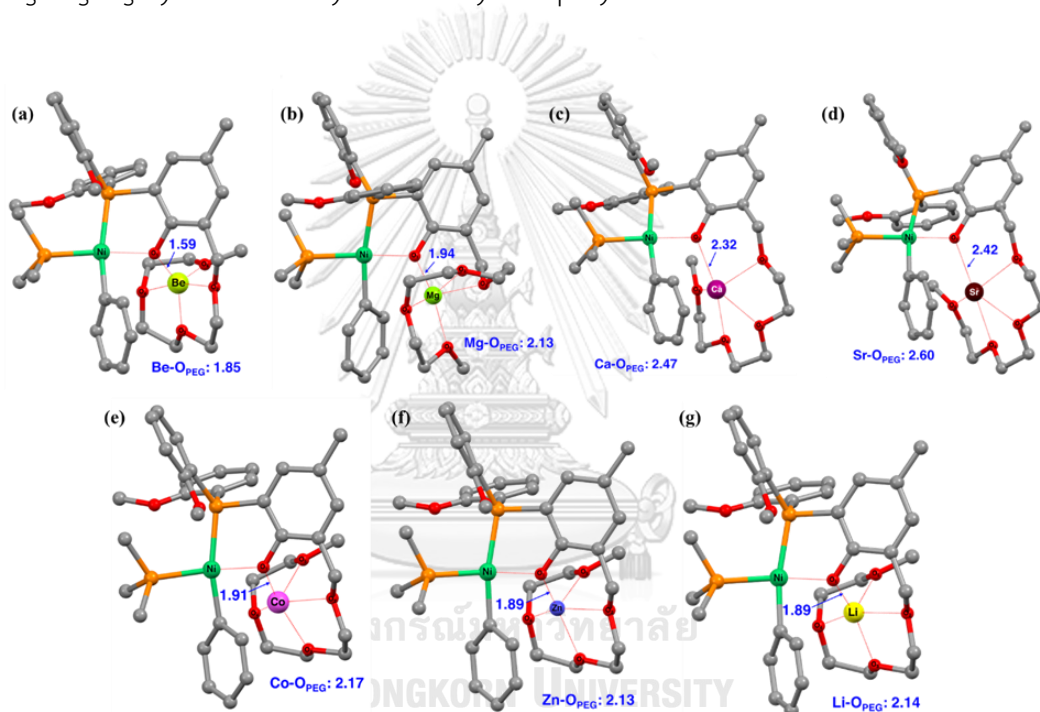


Figure 25 Optimized structures of the Ni-PEG catalysts with (a) Be (b) Mg (c) Ca (d) Sr (e) Co and (f) Zn cation. Their structures were compared with that of the most active (g) Ni-PEG (Li) catalyst. The bond distances (\AA) are given in blue. The H atoms are omitted for clarity.

CHAPTER V

CONCLUSIONS

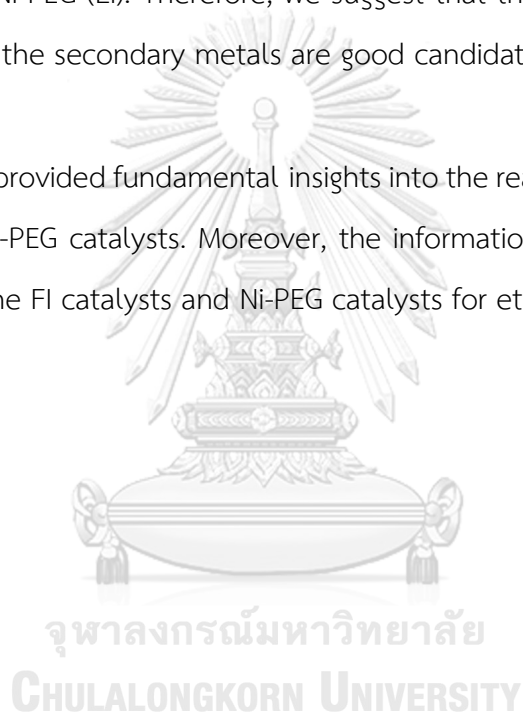
The reaction mechanism of phenoxy-imine (FI) catalysts and nickel phenoxyphosphine polyethylene glycol (Ni-PEG) with different alkali metals (M) for ethylene polymerization was investigated using DFT calculations.

For the FI catalyst, the relative potential energy (RE) of pre-reaction Ti-FI complexes revealed that the rearrangement in *cis*-N/*trans*-O/*cis*-Cl is the most stable form and corresponded to the X-ray structure report. Then, the potential energy profiles of the different groups of IVB transition metals were employed to compare the activation energies with the experimental activities. The obtained results indicate that the second ethylene insertion is the rate-determining (RD) step of this reaction. The activation energy at the RD step (E_a^{RDS}) is Zr-1 < Hf-1 < Ti-1, which shows good agreement with the experimental results. Furthermore, we found that the distance between the transition metal center (M) and nitrogen is possibly related to the catalytic activities. For the effect of ligand substitutions, the Ti-1 system with (O, N) was used as the parent system to compare the E_a^{RDS} and the structural properties with those of the (O, P), (O, O), and (O, S) systems. We found that using P, O, and S instead of N can provide a more potent catalyst than the parent Ti-1 system. Our calculation results suggest that the (O, S) ligand has the most potential to improve catalytic activities because it provides the lowest E_a^{RDS} and the longest Ti-S distance. Moreover, the results obtained from the Ti-3 system exhibited lower E_a^{RDS} , similar to the Ti-1 system. Then, we investigated the Ni-phenoxy-imine (Ni-FI)-based catalyst in octahedral and half Ni-FI in square planar geometries. The results revealed that the nickel (II) complexes based on the half phenoxy-imine (O, N) ligand in the square planar geometry are more reactive than the octahedral geometry.

According to the potential energy profiles of the Ni-PEG catalyst, the isomerization step is required for this reaction. Moreover, the reactant π -complex with

ethylene at *trans* to oxygen provides low activation energy. This finding suggests that the highly active catalyst should have strong interactions with both metal-metal and metal-ligand. Moreover, the catalyst with a less positively charged cation could affect the polymerization rate. The key parameters, which are $M-O_1$ and $M-O_{PEG}$ distances, were found to have a high correlation with the experimental activities, with an $R^2 > 0.8$. Thus, we employed these parameters to design and screen potential candidates for Ni-PEG catalysts. The $M-O_1$ and $M-O_{PEG}$ for the Ni-PEG containing Be, Mg, Co, and Zn are similar to the Ni-PEG (Li). Therefore, we suggest that the Ni-PEG catalysts with Be, Mg, Co, and Zn as the secondary metals are good candidates to produce high-activity catalysts.

This study provided fundamental insights into the reaction mechanisms of both FI catalysts and Ni-PEG catalysts. Moreover, the information provided the design and development of the FI catalysts and Ni-PEG catalysts for ethylene polymerization.



REFERENCES

- [1] K. Kawai, T. Fujita, Discovery and Development of FI Catalysts for Olefin Polymerization: Unique Catalysis and Distinctive Polymer Formation, in: Z. Guan (Ed.), Metal Catalysts in Olefin Polymerization, Springer Berlin Heidelberg, Berlin, Heidelberg, 2009, pp. 3-46.
- [2] H. Makio, H. Terao, A. Iwashita, T. Fujita, FI Catalysts for Olefin Polymerization—A Comprehensive Treatment, Chemical Reviews 111 (2011) 2363-2449.
- [3] T. Yoshida, N. Koga, K. Morokuma, Ab Initio Theoretical Study on Ethylene Polymerization with Homogeneous Silylene-Bridged Group 4 Metallocene Catalysts. Ethylene Insertion and β -Elimination, Organometallics 14 (1995) 746-758.
- [4] Z. Cai, D. Xiao, L.H. Do, Cooperative Heterobimetallic Catalysts in Coordination Insertion Polymerization, Comments on Inorganic Chemistry 39 (2019) 27-50.
- [5] G.H.C. Masson, T.R. Cruz, P.D.S. Gois, D.M. Martins, B.S. Lima-Neto, G.S. Oliveira, A.E.H. Machado, K. Bernardo-Gusmão, B.E. Goi, V.P. Carvalho-Jr, Ruthenium–nickel heterobimetallic complex as a bifunctional catalyst for ROMP of norbornene and ethylene polymerization, New Journal of Chemistry 45 (2021) 11466-11473.
- [6] T.V. Tran, Y.H. Nguyen, L.H. Do, Development of highly productive nickel–sodium phenoxyphosphine ethylene polymerization catalysts and their reaction temperature profiles, Polymer Chemistry 10 (2019) 3718-3721.
- [7] M. Stürzel, S. Mihan, R. Mülhaupt, From Multisite Polymerization Catalysis to Sustainable Materials and All-Polyolefin Composites, Chemical Reviews 116 (2016) 1398-1433.
- [8] P. Corradini, G. Guerra, L. Cavallo, Do New Century Catalysts Unravel the Mechanism of Stereocontrol of Old Ziegler–Natta Catalysts?, Accounts of Chemical Research 37 (2004) 231-241.
- [9] J. Kumawat, V.K. Gupta, Fundamental aspects of heterogeneous Ziegler–Natta olefin polymerization catalysis: an experimental and computational overview, Polymer Chemistry 11 (2020) 6107-6128.

- [10] V.H. Nissinen, M. Linnolahti, A.S. Bazhenov, T.T. Pakkanen, T.A. Pakkanen, P. Denifl, T. Leinonen, K. Jayaratne, A. Pakkanen, Polyethylenimines: Multidentate Electron Donors for Ziegler–Natta Catalysts, *The Journal of Physical Chemistry C* 121 (2017) 23413-23421.
- [11] P. Pokasermson, P. Praserttham, Comparison of activity of Ziegler-Natta catalysts prepared by recrystallization and chemical reaction methods towards polymerization of ethylene, *Engineering Journal* 13 (2009) 57-64.
- [12] A. Shamiri, M.H. Chakrabarti, S. Jahan, M.A. Hussain, W. Kaminsky, P.V. Aravind, W.A. Yehye, The Influence of Ziegler-Natta and Metallocene Catalysts on Polyolefin Structure, Properties, and Processing Ability, *Materials (Basel)* 7 (2014) 5069-5108.
- [13] W. Kaminsky, Highly active metallocene catalysts for olefin polymerization, *Journal of the Chemical Society, Dalton Transactions* (1998) 1413-1418.
- [14] H.G. Alt, Self-immobilizing catalysts and cocatalysts for olefin polymerization, *Dalton Transactions* (2005) 3271-3276.
- [15] E.Y. Hwang, G.H. Park, C.S. Lee, Y.Y. Kang, J. Lee, B.Y. Lee, Preparation of octahydro- and tetrahydro-[1,10]phenanthroline zirconium and hafnium complexes for olefin polymerization, *Dalton Transactions* 44 (2015) 3845-3855.
- [16] M.C. Baier, M.A. Zuideveld, S. Mecking, Post-Metallocenes in the Industrial Production of Polyolefins, *Angewandte Chemie International Edition* 53 (2014) 9722-9744.
- [17] T. Matsugi, T. Fujita, High-performance olefin polymerization catalysts discovered on the basis of a new catalyst design concept, *Chemical Society Reviews* 37 (2008) 1264-1277.
- [18] H. Makio, N. Kashiwa, T. Fujita, FI Catalysts: A New Family of High Performance Catalysts for Olefin Polymerization, *Advanced Synthesis & Catalysis* 344 (2002) 477-493.
- [19] M. Mitani, J. Saito, S.-i. Ishii, Y. Nakayama, H. Makio, N. Matsukawa, S. Matsui, J.-i. Mohri, R. Furuyama, H. Terao, H. Bando, H. Tanaka, T. Fujita, FI Catalysts: new olefin polymerization catalysts for the creation of value-added polymers, *The Chemical Record* 4 (2004) 137-158.
- [20] D. Das, S.S. Mohapatra, S. Roy, Recent advances in heterobimetallic catalysis across a “transition metal–tin” motif, *Chemical Society Reviews* 44 (2015) 3666-3690.
- [21] R.M. Haak, S.J. Wezenberg, A.W. Kleij, Cooperative multimetallic catalysis using metallocenes, *Chemical Communications* 46 (2010) 2713-2723.

- [22] T.V. Tran, L.J. Karas, J.I. Wu, L.H. Do, Elucidating Secondary Metal Cation Effects on Nickel Olefin Polymerization Catalysts, *ACS Catalysis* 10 (2020) 10760-10772.
- [23] Y.V. Kissin, R.I. Mink, T.E. Nowlin, A.J. Brandolini, Ethylene polymerization reactions with Ziegler–Natta catalysts. III. Chain-end structures and polymerization mechanism, *Journal of Polymer Science Part A: Polymer Chemistry* 37 (1999) 4281-4294.
- [24] C.P. Gordon, S. Shirase, K. Yamamoto, R.A. Andersen, O. Eisenstein, C. Copéret, NMR chemical shift analysis decodes olefin oligo- and polymerization activity of d^0 group 4 metal complexes, *Proceedings of the National Academy of Sciences* 115 (2018) E5867–E5876.
- [25] S.V. Nikitin, V.V. Nikitin, I.I. Oleynik, I.V. Oleynik, E.G. Bagryanskaya, Activity of phenoxy-imine titanium catalysts in ethylene polymerization: A quantum chemical approach, *Journal of Molecular Catalysis A: Chemical* 423 (2016) 285-292.
- [26] H. Terao, A. Iwashita, N. Matsukawa, S. Ishii, M. Mitani, H. Tanaka, T. Nakano, T. Fujita, Ethylene and Ethylene/ α -Olefin (Co)Polymerization Behavior of Bis(phenoxy–imine)Ti Catalysts: Significant Substituent Effects on Activity and Comonomer Incorporation, *ACS Catalysis* 1 (2011) 254-265.
- [27] S. Damavandi, N. Samadieh, S. Ahmadjo, Z. Etemadinia, G.H. Zohuri, Novel Ni-based FI catalyst for ethylene polymerization, *European Polymer Journal* 64 (2015) 118-125.
- [28] P. Chasing, P. Maitarad, H. Wu, D. Zhang, L. Shi, V. Promarak, Straightforward Design for Phenoxy-Imine Catalytic Activity in Ethylene Polymerization: Theoretical Prediction, *Catalysts* 8 (2018).
- [29] Z. Cai, D. Xiao, L.H. Do, Fine-Tuning Nickel Phenoxyimine Olefin Polymerization Catalysts: Performance Boosting by Alkali Cations, *Journal of the American Chemical Society* 137 (2015) 15501-15510.
- [30] D. Zhang, C. Chen, Influence of Polyethylene Glycol Unit on Palladium- and Nickel-Catalyzed Ethylene Polymerization and Copolymerization, *Angewandte Chemie International Edition* 56 (2017) 14672-14676.
- [31] J.E. House, Chapter 1 - Origins of Quantum Theory, in: J.E. House (Ed.), *Fundamentals of Quantum Mechanics (Third Edition)*, Academic Press 2018, pp. 1-22.

- [32] E. Schrödinger, An Undulatory Theory of the Mechanics of Atoms and Molecules, *Physical Review* 28 (1926) 1049-1070.
- [33] J.M. Combes, P. Duclos, R. Seiler, The Born-Oppenheimer Approximation, in: G. Velo, A.S. Wightman (Eds.), *Rigorous Atomic and Molecular Physics*, Springer US, Boston, MA, 1981, pp. 185-213.
- [34] C.D. Sherrill, An introduction to Hartree-Fock molecular orbital theory, School of Chemistry and Biochemistry Georgia Institute of Technology (2000).
- [35] E.K. Gross, R.M. Dreizler, *Density functional theory*, Springer Science & Business Media 2013.
- [36] K. Burke, Perspective on density functional theory, *The Journal of Chemical Physics* 136 (2012) 150901.
- [37] P. Geerlings, F. De Proft, W. Langenaeker, Conceptual Density Functional Theory, *Chemical Reviews* 103 (2003) 1793-1874.
- [38] M.T. Lusk, A.E. Mattsson, High-performance computing for materials design to advance energy science, *MRS Bulletin* 36 (2011) 169-174.
- [39] A.J. Cohen, P. Mori-Sánchez, W. Yang, Challenges for Density Functional Theory, *Chemical Reviews* 112 (2012) 289-320.
- [40] S. Kurth, M.A.L. Marques, E.K.U. Gross, *Density-Functional Theory*, in: F. Bassani, G.L. Liedl, P. Wyder (Eds.), *Encyclopedia of Condensed Matter Physics*, Elsevier, Oxford, 2005, pp. 395-402.
- [41] W. Kohn, L.J. Sham, Self-Consistent Equations Including Exchange and Correlation Effects, *Physical Review* 140 (1965) A1133-A1138.
- [42] J.R. Chelikowsky, Nanostructures, Electronic Structure of, in: F. Bassani, G.L. Liedl, P. Wyder (Eds.), *Encyclopedia of Condensed Matter Physics*, Elsevier, Oxford, 2005, pp. 51-58.
- [43] E. Nakamachi, H. Hwang, Y. Uetsuji, H. Kuramae, Three-scale process-crystallographic analysis of a new biocompatible piezoelectric material MgSiO_3 generation, 2010 2nd International Conference on Computer Technology and Development, 2010, pp. 206-210.

- [44] R. Peverati, D.G. Truhlar, Exchange–Correlation Functional with Good Accuracy for Both Structural and Energetic Properties while Depending Only on the Density and Its Gradient, *Journal of Chemical Theory and Computation* 8 (2012) 2310-2319.
- [45] K.L. Schuchardt, B.T. Didier, T. Elsethagen, L. Sun, V. Gurumoorthi, J. Chase, J. Li, T.L. Windus, Basis Set Exchange: A Community Database for Computational Sciences, *Journal of Chemical Information and Modeling* 47 (2007) 1045-1052.
- [46] J.E. House, Chapter 14 - Comments on Computational Methods, in: J.E. House (Ed.), *Fundamentals of Quantum Mechanics (Third Edition)*, Academic Press 2018, pp. 335-347.
- [47] E. Zurek, T. Ziegler, Theoretical studies of the structure and function of MAO (methylaluminoxane), *Progress in Polymer Science* 29 (2004) 107-148.
- [48] M.E.Z. Velthoen, A. Muñoz-Murillo, A. Bouhmadi, M. Cecius, S. Diefenbach, B.M. Weckhuysen, The Multifaceted Role of Methylaluminoxane in Metallocene-Based Olefin Polymerization Catalysis, *Macromolecules* 51 (2018) 343-355.
- [49] S. Escayola, A. Brotons-Rufes, N. Bahri-Laleh, F. Ragone, L. Cavallo, M. Solà, A. Poater, Fluxional bis(phenoxy-imine) Zr and Ti catalysts for polymerization, *Theoretical Chemistry Accounts* 140 (2021) 49.
- [50] M.J. Frisch, G.W. Trucks, H.B. Schlegel, G.E. Scuseria, M.A. Robb, J.R. Cheeseman, G. Scalmani, V. Barone, G.A. Petersson, H. Nakatsuji, X. Li, M. Caricato, A.V. Marenich, J. Bloino, B.G. Janesko, R. Gomperts, B. Mennucci, H.P. Hratchian, J.V. Ortiz, A.F. Izmaylov, J.L. Sonnenberg, Williams, F. Ding, F. Lipparini, F. Egidi, J. Goings, B. Peng, A. Petrone, T. Henderson, D. Ranasinghe, V.G. Zakrzewski, J. Gao, N. Rega, G. Zheng, W. Liang, M. Hada, M. Ehara, K. Toyota, R. Fukuda, J. Hasegawa, M. Ishida, T. Nakajima, Y. Honda, O. Kitao, H. Nakai, T. Vreven, K. Throssell, J.A. Montgomery Jr., J.E. Peralta, F. Ogliaro, M.J. Bearpark, J.J. Heyd, E.N. Brothers, K.N. Kudin, V.N. Staroverov, T.A. Keith, R. Kobayashi, J. Normand, K. Raghavachari, A.P. Rendell, J.C. Burant, S.S. Iyengar, J. Tomasi, M. Cossi, J.M. Millam, M. Klene, C. Adamo, R. Cammi, J.W. Ochterski, R.L. Martin, K. Morokuma, O. Farkas, J.B. Foresman, D.J. Fox, *Gaussian 09 Rev. D.01*, Wallingford, CT, 2016.
- [51] T.H. Dunning, Gaussian basis sets for use in correlated molecular calculations. I. The atoms boron through neon and hydrogen, *The Journal of Chemical Physics* 90 (1989) 1007-1023.

- [52] P.J. Hay, W.R. Wadt, Ab initio effective core potentials for molecular calculations. Potentials for the transition metal atoms Sc to Hg, *The Journal of Chemical Physics* 82 (1985) 270-283.
- [53] A.V. Marenich, C.J. Cramer, D.G. Truhlar, Universal Solvation Model Based on Solute Electron Density and on a Continuum Model of the Solvent Defined by the Bulk Dielectric Constant and Atomic Surface Tensions, *The Journal of Physical Chemistry B* 113 (2009) 6378-6396.
- [54] T. Kuamit, M. Ratanasak, C. Rungnim, V. Parasuk, Effects of shape, size, and pyrene doping on electronic properties of graphene nanoflakes, *Journal of Molecular Modeling* 23 (2017) 355.
- [55] Y. Zhao, D.G. Truhlar, The M06 suite of density functionals for main group thermochemistry, thermochemical kinetics, noncovalent interactions, excited states, and transition elements: two new functionals and systematic testing of four M06-class functionals and 12 other functionals, *Theoretical Chemistry Accounts* 120 (2008) 215-241.
- [56] S. Noda, A. Nakamura, T. Kochi, L.W. Chung, K. Morokuma, K. Nozaki, Mechanistic Studies on the Formation of Linear Polyethylene Chain Catalyzed by Palladium Phosphine–Sulfonate Complexes: Experiment and Theoretical Studies, *Journal of the American Chemical Society* 131 (2009) 14088-14100.
- [57] M.J. Frisch, G.W. Trucks, H.B. Schlegel, G.E. Scuseria, M.A. Robb, J.R. Cheeseman, G. Scalmani, V. Barone, G.A. Petersson, H. Nakatsuji, X. Li, M. Caricato, A.V. Marenich, J. Bloino, B.G. Janesko, R. Gomperts, B. Mennucci, H.P. Hratchian, J.V. Ortiz, A.F. Izmaylov, J.L. Sonnenberg, Williams, F. Ding, F. Lipparini, F. Egidi, J. Goings, B. Peng, A. Petrone, T. Henderson, D. Ranasinghe, V.G. Zakrzewski, J. Gao, N. Rega, G. Zheng, W. Liang, M. Hada, M. Ehara, K. Toyota, R. Fukuda, J. Hasegawa, M. Ishida, T. Nakajima, Y. Honda, O. Kitao, H. Nakai, T. Vreven, K. Throssell, J.A. Montgomery Jr., J.E. Peralta, F. Ogliaro, M.J. Bearpark, J.J. Heyd, E.N. Brothers, K.N. Kudin, V.N. Staroverov, T.A. Keith, R. Kobayashi, J. Normand, K. Raghavachari, A.P. Rendell, J.C. Burant, S.S. Iyengar, J. Tomasi, M. Cossi, J.M. Millam, M. Klene, C. Adamo, R. Cammi, J.W. Ochterski, R.L. Martin, K. Morokuma, O. Farkas, J.B. Foresman, D.J. Fox, Gaussian 16 Rev. C.01, Wallingford, CT, 2016.

- [58] J.-D. Chai, M. Head-Gordon, Long-range corrected hybrid density functionals with damped atom–atom dispersion corrections, *Physical Chemistry Chemical Physics* 10 (2008) 6615-6620.
- [59] K.E. Riley, K.-A. Tran, P. Lane, J.S. Murray, P. Politzer, Comparative analysis of electrostatic potential maxima and minima on molecular surfaces, as determined by three methods and a variety of basis sets, *Journal of Computational Science* 17 (2016) 273-284.
- [60] A. Posada-Borbón, A. Posada-Amarillas, Theoretical DFT study of homonuclear and binary transition-metal dimers, *Chemical Physics Letters* 618 (2015) 66-71.
- [61] A.E. Reed, F. Weinhold, Natural bond orbital analysis of near-Hartree–Fock water dimer, *The Journal of Chemical Physics* 78 (1983) 4066-4073.
- [62] S. Matsui, M. Mitani, J. Saito, Y. Tohi, H. Makio, N. Matsukawa, Y. Takagi, K. Tsuru, M. Nitabaru, T. Nakano, H. Tanaka, N. Kashiwa, T. Fujita, A Family of Zirconium Complexes Having Two Phenoxy–Imine Chelate Ligands for Olefin Polymerization, *Journal of the American Chemical Society* 123 (2001) 6847-6856.
- [63] R. Lapenta, A. Buonerba, E. Luciano, F. Della Monica, A. De Nisi, M. Monari, A. Grassi, C. Capacchione, S. Milione, Phenylene-Bridged OSSO-Type Titanium Complexes in the Polymerization of Ethylene and Propylene, *ACS Omega* 3 (2018) 11608-11616.
- [64] M. Ratanasak, J. Hasegawa, V. Parasuk, Roles of Salicylate Donors in Enhancement of Productivity and Isotacticity of Ziegler–Natta Catalyzed Propylene Polymerization, *Polymers* 12 (2020).
- [65] W.H. Sun, D. Zhang, S. Zhang, S. Jie, J. Hou, Ethylene polymerization promoted by nickel complexes, *Kinetics and Catalysis* 47 (2006) 278-283.
- [66] A. Michalak, T. Ziegler, Polymerization of Ethylene Catalyzed by a Nickel(+2) Anilinetropone-Based Catalyst: DFT and Stochastic Studies on the Elementary Reactions and the Mechanism of Polyethylene Branching, *Organometallics* 22 (2003) 2069-2079.
- [67] A. Zeller, T. Strassner, The mechanism of ethylene polymerization by nickel salicylaldiminato catalysts – Agostic interactions and their kinetic isotope effects, *Journal of Organometallic Chemistry* 691 (2006) 4379-4385.

- [68] M.S.W. Chan, L. Deng, T. Ziegler, Density Functional Study of Neutral Salicylaldiminato Nickel(II) Complexes as Olefin Polymerization Catalysts, *Organometallics* 19 (2000) 2741-2750.
- [69] D.G. Musaev, M. Svensson, K. Morokuma, S. Strömberg, K. Zetterberg, P.E.M. Siegbahn, Density Functional Study of the Mechanism of the Palladium(II)-Catalyzed Ethylene Polymerization Reaction, *Organometallics* 16 (1997) 1933-1945.
- [70] M. Ratanasak, T. Rungrotmongkol, O. Saengsawang, S. Hannongbua, V. Parasuk, Towards the design of new electron donors for Ziegler–Natta catalyzed propylene polymerization using QSPR modeling, *Polymer* 56 (2015) 340-345.
- [71] D. Xiao, Z. Cai, L.H. Do, Accelerating ethylene polymerization using secondary metal ions in tetrahydrofuran, *Dalton Transactions* 48 (2019) 17887-17897.



VITA

NAME Pavée Apilardmongkol(Pongsajanukul)

DATE OF BIRTH 27 June 1991

PLACE OF BIRTH Bangkok

INSTITUTIONS ATTENDED 2017 – present: Doctor of Philosophy (Ph.D.) in Physical Chemistry, Department of Chemistry, Faculty of Science, Chulalongkorn University, Bangkok, Thailand
2014 – 2016: Master of Science (M.Sc.) in Physical Chemistry, Department of Chemistry, Faculty of Science, Chulalongkorn University, Bangkok, Thailand
2010 – 2013: Bachelor of Science (B.Sc.), Department of Chemistry, Faculty of Science, Khon Kaen University, Khon Kaen, Thailand (Second-Class honors)
2004 – 2009: Secondary School, Surawittayakarn school, Surin, Thailand

HOME ADDRESS 126,128 Tedsabarn 3 Road, Muang Surin District, Surin, Thailand 32000

PUBLICATION P. Pongsajanukul, V. Parasuk, S. Fritzsche, S. Assabumrungrat, S. Wongsakulphasatch, T. Bovornratanaraks, T. Chokbunpjam. Theoretical study of carbon dioxide adsorption and diffusion in MIL-127(Fe) metal organic framework. Chemical Physics 2017, 491, 118–125.

AWARD RECEIVED 2019 Outstanding Student Poster Award at the Pure and Applied Chemistry International Conference (PACCON)
2016 Best Poster Award – Third place at the 13th Thai Summer School of Computational Chemistry